Effective Earth Radius Factor (the k-factor) Distribution for Southern Africa

By

Odedina Peter Kemi

A Dissertation Submitted in Part Fulfillment of the Requirement for the Degree of

Masters in Electrical Engineering in Telecommunications and Information Technology

University of KwaZulu-Natal

School of Engineering

Centre of Excellence in Radio Access and Rural Technologies

February 2005

Supervised by Professor T J Afullo

DISSERTATION TITLE

Effective Earth Radius Factor (the k-factor) Distribution for Southern Africa

SUBMITTED BY

Odedina Peter Kemi

IN PARTIAL FULFILLMENT OF THE DEGREE

Masters in Electrical Engineering in Telecommunications and Information Technology
From the University of KwaZulu-Natal (Westville Campus)

DATE OF SUBMISSION

February 2005

SUPERVISED BY

Professor T.J. Afullo

As the candidate's supervisor, I have approved this dissertation for submission.

Signed: _____

Name: T. J. AFULLO Date: 01/04/2005

DECLARATION

I, Odedina Peter Kemi, Student Number 200302084, hereby declare that the dissertation entitled Effective Earth Radius Factor (k-factor) Distribution for Southern Africa is a result of my own investigation and present my work unless specifically referenced in the text. This work has not been submitted in part or in full for any degree to any university.

Signed:_____

Name :_____ Date :_____

ACKNOWLEDGEMENTS

To God is the glory for given me the strength to complete this work. Also I thank my brothers Mr. Joe Odedina and Mr. Gabriel Odedina for their financial and moral Support.

I will like to specially thank my able supervisor Prof. T.J.O Afullo for painstakingly going through the report several times and his constructive criticisms, his patience is highly appreciated.

I sincerely appreciate the contribution of Amith S. Dabideen by releasing the Durban data collected from the South African Weather Service used in the dissertation.

My sincere gratitude to all the academic staffs in the department such as Mr. Rathi Sewsunker, Pro. A.M. Chol, Prof. B. Nleya, for their moral support and professional advise throughout the research period.

Also appreciated is the effort and assistance of the administrator Mrs. René Truter, for her moral support during the research period.

I thank my dearest wife Mrs. Bunmi Odedina for her words of encouragement, understanding and emotional support during the research period and finally I appreciate the support of my dear friend and colleague Pius Adewale Owolawi.

ABSTRACT

Proper radio link design requires an accurate prediction of the effective earth radius factor (the k-factor) distribution, for the location where propagation is intended. Though a median value of k equals 4/3 is normally use for communication design purposes, in reality the true k-factor values differ, for different locations, globally.

The effective earth radius factor distribution for Southern Africa was evaluated in the dissertation. The two Southern African countries chosen for the study are Botswana and Republic of South Africa. The dissertation reports in detail a study on the topic using three years radiosonde data obtain in Maun, Botswana and ten months radiosonde data collected in Durban, South Africa.

An analytical model was proposed, which predicts the probability density function of the k-factor for the Southern Africa using the data from these two countries. Also a comparison of the data from the two countries was done in the analysis and reported in the write-up.

The application of the work was also investigated and reported by simulating a radio link between Sherwood and Umlazi in KwaZulu-Natal Province of South Africa. The consequence of using inappropriate design value of k on link reliability was also investigated and reported.

Recommendation for future work was given in the concluding chapter for future improvement on the study. Radio communication designers will find the results obtain in the report useful.

TABLE OF CONTENTS

LIST OF FIGURES

LIST OF TABLES

CHAPTER ONE

1.0 Introduction

The two mechanisms of importance in radio link design are refraction and diffraction. The first of these two mechanisms gives rise to the k-factor, which is instrumental in causing the Earth to bulge up and cause obstruction fading. When the atmosphere is sufficiently sub-refractive, the radio wave signal will be bent in such a way that the earth bulge appears to obstruct the direct path between the transmitter and receiver.

All electromagnetic waves are refracted when they pass from a material of one refractive index to another. In the atmosphere, the changes in refractive index are at most times gradual, since the density of the air decreases with height, theoretically at a uniform rate. The general vertical changes in refractive index of the atmosphere produce a curving of the waves in the vertical plane as they travel from the transmitter to the receiver. The amount of path curvature varies with time due to changes in temperature, pressure and humidity. Under normal propagation conditions, the path curves away from true Earth's surface so that the radio horizon is effectively extended. Good radio link design prevents this from happening by ensuring that the line of sight from the transmitter and receiver is rarely lost under worst refractivity conditions.

The data used in this dissertation were gathered in Maun, Botswana for three years (1996-1998) and in Durban, South Africa for 10 months (Nov 2003 – Aug 2004). The data was gathered by launching a radiosonde in the troposphere twice daily (1:00 a.m. 1:00p.m). Our proposed model was developed based on this data. We start by briefly reviewing the climatic and seasonal features of Botswana and South Africa.

1.1 Botswana Climate and Seasonal Features

Botswana is a land-locked country, bordered by Namibia to the west and north, Zimbabwe to the north-east, and Republic of South Africa to the south and south-east [1]. It occupies 582,000 sq. km. of the Kalahari basin, with an average altitude of about 900m above sea level. It is characterised by gentle undulations to flat surfaces, consisting of Kalahari sands overlying Archean rocks in most part of the country. However the east is more hilly and broken. Most of Botswana is without surface drainage and apart from the bordering Chobe and Limpopo rivers the rest of the country's drainage does not reach the sea [1]. Flowing into the north-west from the Angolan highlands is the perennial Okavango River. The Okavango drains into a depression in

the plateau, to form the Okavango swamps and the ephemeral lake Ngami. From this vast marsh covering 16,000 sq. km, there is a seasonal flow of water into River Xau and Makgadikgadi salt pans [2]. Most of the water brought into Botswana by the Okavango is lost through evaporation and transpiration in the swamps. The Kalahari Desert dominates southern and western Botswana. From the near-desert conditions of the south-west with an average annual rainfall around 130 mm, there is a gradual increase in precipitation towards the north (635 mm) and the east (400 – 500 mm) [2]. There is an associated transition in vegetation from the sparse thorn-veld of the Kalahari Desert to the dry woodland Savannah of the north and east; and the infertile sands give way eastwards to better soils developed on granitic and sedimentary rocks. The rainy season in Botswana occurs during the summer months. It begins in October with peak in December and end in March. Summer temperatures range from 20°C in the night to 40°C at mid-afternoon. The winter season begins towards end of May and ends in August. Winter temperatures range from as high as 20°C during the afternoons, to below freezing point at night [2]. The Map of Botswana and the neighbouring countries is shown in Fig. 1.1.

Fig. 1.1 Map of Botswana and Neighbouring Countries

1.2 South Africa Climate and Physical Features

South Africa is situated at the southern tip of the continent of Africa, it is rich in climate and has unique physical features such as the costal belts, highland caves sea, rich loamy soil, etc. It has a total area of 1,219,912 sq km. South Africa borders other countries like Botswana and Zimbabwe in the central north, Mozambique in north-east, Namibia in north-west. Swaziland and Lesotho are embedded in the country (see Fig. 1.2). The Southern parts of the country are bordered by the Indian Ocean and the Atlantic Ocean. South Africa has a coastline of 2,798 km; the highest point of South Africa is Njesuthi (3,408 m) with the lowest point being the Atlantic Ocean (0 m).

The climate varies with regions but it is mostly semi-arid subtropical along east coast sunny days and cool nights. The terrain is mostly vast interior plateau rimmed by rugged hills and narrow coastal plains. The only natural hazard of South Africa is its prolonged droughts.

Fig 1.2 Map of South Africa and Neighbouring Countries

One of the greenest and best loamy areas of the country is KwaZulu-Natal, which is only 7.6% of the country and the second most populous province. Lying in a broad strip with the Indian Ocean as its western border, it borders Swaziland and Mozambique to the north. Its western border is

marked by the dramatic Drakensberg mountain ranges, which have several peaks, well over 3 000m, and its topography combines mountainous areas, rugged green hills and deep-cut valleys.

Between the mountains and the humid, subtropical coastline is savannah grassland, but there are also areas of indigenous forest here and along the coast. The largest of its many rivers is the Tugela. It is a summer rainfall area, with a climate that ranges from extremely hot along the coast in summer to heavy snow on the mountains in winter. The Midlands are drier than the coast and can be very cold in winter.

KwaZulu-Natal has two capitals: Pietermaritzburg (the province's second-largest city) and Ulundi (the traditional capital) in the north; these two capitals are both inland. The largest city in KwaZulu-Natal is Durban.

South Africa's two biggest harbours are situated in Durban and Richard's Bay - the latter a comparatively small town, its harbour specialising in bulk exports, especially coal which is mined in the interior. Heavy minerals are mined at Richard's Bay. Durban's is the busiest port in sub-Saharan Africa.

The fertility of the soil and comparatively good rainfall (more than 1 000 mm a year) make agriculture central to the economy. Sugar-cane and tropical fruits are major products of the coastal belt. Dairy, stock and vegetable farming are important land usage, so is forestry and tea plantations.

Temperatures in Durban are mild in winter and warm to hot in summer. The mean annual temperature is 20.4°C and the annual range is 8.0°C. Highest mean temperatures are experienced in February and lowest mean temperatures in July. The maximum temperatures occur in October in association with Berg wind conditions. Temperature is highly variable in any particular area of Durban as a result of topography, type of surface cover and artificial heat production due to combustion activities in industries and motor vehicles.

1.3 The Atmosphere

The atmosphere is a mixture of gases and vapours which are most dense at sea level. The atmosphere is divided into different layers according to the variability of the temperature gradient with altitude. These layers are the troposphere, stratosphere, mesosphere and ionosphere. The

variation of these layers with altitude is shown in Fig 1.3. The boundaries of the layers are referred to as pauses with an identifying prefix [3].

Upon examination, the atmosphere is found to be a complex system not a simple chemical nor even a compound, but a relatively stable mixture of a number of gases [4]. First, there are several chemical elements, which remain permanently in gaseous form under all natural conditions. Secondly gaseous water known as water vapour is a variable part of this mixture. Under certain conditions liquid and solid forms of water also occur in the air but these are not included in the definition of air. Finally, the air always contains but not as essential ingredients a great number of solid particles of variable natures known collectively as dust.

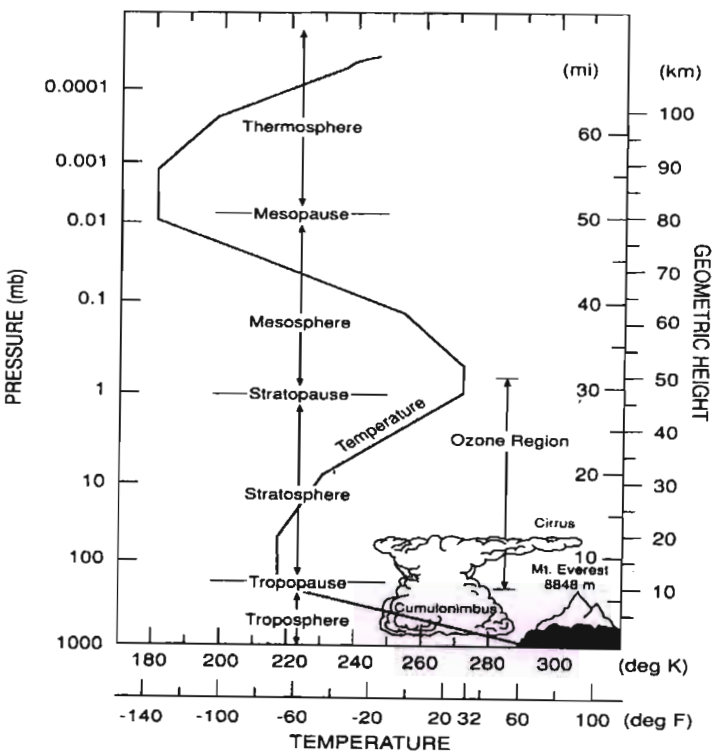

Fig. 1.3 Generalized Vertical Distribution of Temperature and Pressure up to 110 km [3].

1.3.1 The Troposphere

The lowest layer of the atmosphere is called the troposphere. It is the zone where weather phenomenon and atmospheric turbulence are most marked, and it contains 75 per cent of the total molecular or gaseous mass of the atmosphere and virtually all the water vapour and aerosols.

Throughout this layer there is a general decrease of temperature with height at a mean rate of about 6.5°C/km and the whole zone is capped in most places by a temperature inversion level[1] and in others by a zone that is isothermal with height [4]. The troposphere thus remains to a large extent, self-contained because the inversion acts as a 'lid', which effectively limits convection. This inversion level or weather ceiling is called the tropopause (Fig. 1.4). Its height is not constant either in space or time. It seems that the height of the tropopause at any point is correlated with sea-level temperature and pressure which are in turn related to the factors of latitude, season and daily changes in surface pressure [4].

1.3.2 Stratosphere

The second major atmospheric layer is the stratosphere, which extends upwards from the tropopause to about 50km. Although the stratosphere contains much of the total atmospheric ozone[2], the maximum temperatures associated with the absorption of the sun's ultraviolet radiation by ozone occur at the stratopause, where temperatures may exceed 0°C (Fig. 1.4). The air density is much less in the stratosphere so that even limited absorption produces a large temperature increase. Temperature increases fairly generally with height in summer with the coldest air at the equatorial tropopause. In winter the structure is more complex with very low temperatures averaging -80°C [4].
Similar low temperatures are found in the middle stratosphere at high latitude, whereas over 50° – 60°N there is a marked warm region with nearly isothermal conditions at about -45°C to -50°C.

1.4 Dust

The gases of the atmosphere maintain in suspension an immense number of nongaseous substances of various kinds, which are collectively called dust. In addition to the visible dust, which sometimes fills the air and darkens the sun in dry regions, the air always or nearly always carries small particles of organic matter such as seeds, spores and bacteria. Much more numerous however are the macroscopic inorganic particles which contribute to the formation of haze, clouds and precipitation [4]. Some of these are fine particles of soil or of smoke or salt from ocean spray, which are lifted and diffused by the winds and rising air currents. The dust is

[1] a layer of relatively warm air above a colder one, an increased temperature with height.

[2] it reaches a peak density at approximately 22km

naturally denser in the lower atmosphere but it is carried to heights of up to several kilometers. Large numbers of even finer particles are thrown into the air by volcanic explosions and many more result from the burning of meteors in the upper air, thus furnishing a supply of dust to the air at great heights.

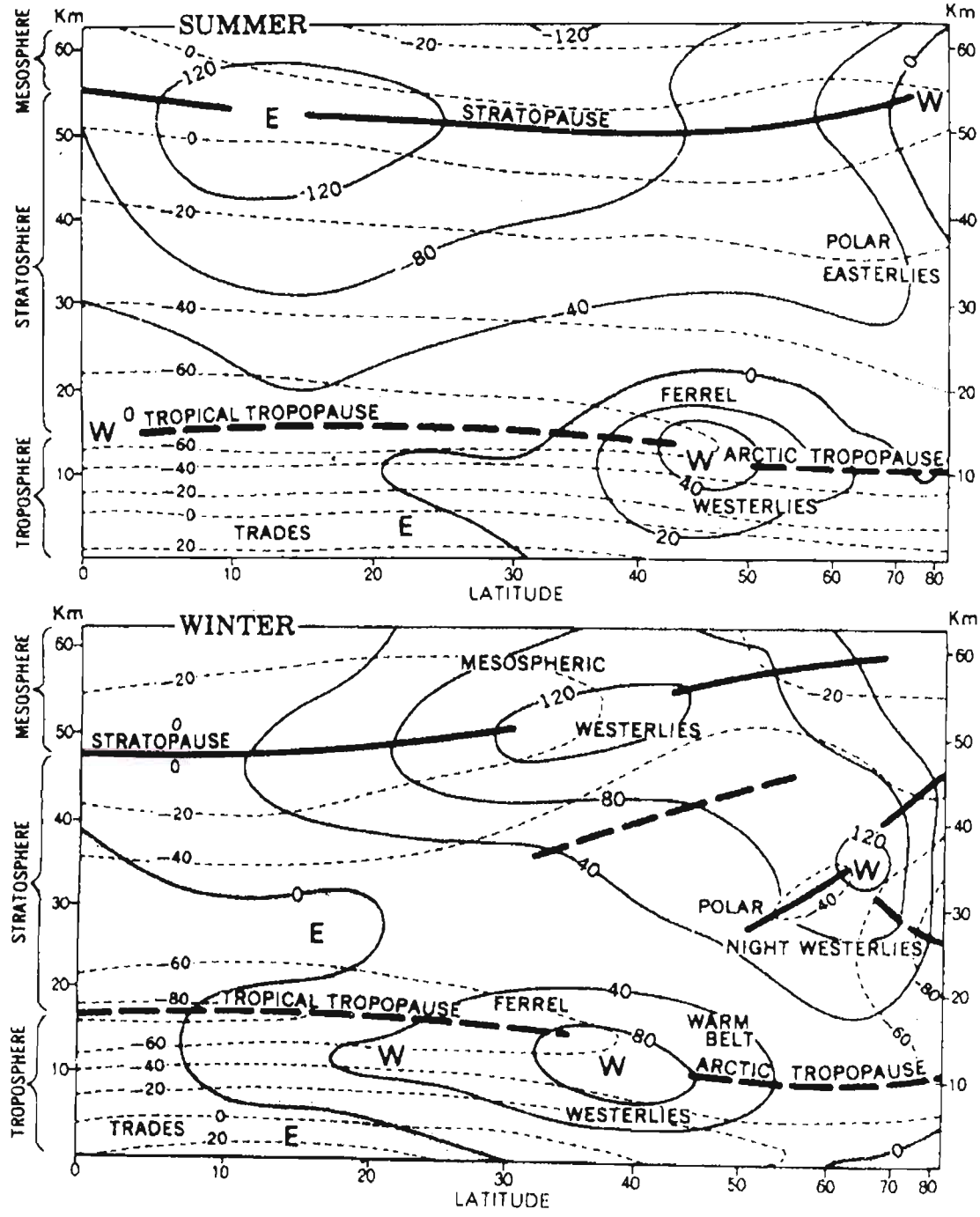

Fig. 1.4 Mean Zonal (westerly) winds and Temperatures showing the broken Tropopause near the mean Ferrel jet stream [4].

Many of these particles are very minute but they have two important effects on the weather. Firstly, many of them are water-absorbent and are nuclei on which water vapour begins. Secondly, they intercept some of the heat coming from the sun. When there is an unusual amount of such dust as in time of great volcanic activity, the result may be to reduce the average temperature of the globe. Dust plays a part in the creation of the varied colours of sunrise and sunset. For three years after the violent explosion of the volcano, Krakatoa in the East Indies in 1883, brilliant twilight colours were seen around the world as the dust gradually spread from its source until it encircled the globe [4]. In mid-ocean, the air has been found to contain from 500 to 2,000 of these microscopic and sub-microscopic dust particles per cubic centimeter and in dusty cities more than 100,000 per cubic centimeter. Current rain-making and weather-control theories now being tested are based on the importance of these hygroscopic dust particles to the weather processes.

1.5 Water Vapour

Water vapour is contributed to the air by evaporation from water surfaces, soil and living tissues and by combustion [4]. It is an important constituent of the atmosphere but unlike the other gases, it is quite variable in amount, ranging from a minute proportion in the air of desert and polar regions to a maximum of approximately 4% by volume in the warm humid tropics. Some water remains in the air as a gas at all temperatures; but the amount that may be mixed with the other gases of the air at low temperatures is small compared with the possible amount when the temperature is high. The importance of atmospheric moisture to all forms of life is universally recognized. However, less well known is the very important role which it plays in the physical processes of the atmosphere and the impact on radio propagation [4].

1.5.1 Humidity

Some of the molecules at the surface of a liquid are continually escaping and entering the air as gaseous molecules thereby reducing the volume of the liquid. For any surface of a given liquid, such as water, the number of molecules that escape in a particular period of time depends solely upon the speed at which they are moving, that is, upon the temperature of the surface of the liquid. Raising the temperature increases the velocity of the molecules and the rate at which they break free from the liquid surface. In this way, water vapour enters the air from water surfaces, moist soil, and growing plants. This process is called evaporation and it occurs in all liquids. Ice

and snow sometimes change directly from the solid to the gaseous state. This process is called sublimation. In breaking away from the attraction of the other molecules, the escaping molecules use heat energy at the expense of the immediate environment. The heat energy so lost does not warm the gas but is used solely in effecting the change of state and is called latent heat of vaporization or latent heat of sublimation as the case may be. This latent heat is again returned to the environment upon condensation of the water vapour. The wide use of evaporative cooling units throughout the western half of the United States is evidence that cooling by evaporation contributes much to the temperature characteristics of the atmosphere.

1.5.1.1 Absolute Humidity

In dealing with the moisture in the air, one quantity that may be measured is the actual mass of water vapour in a given sample of air. It may be expressed, for example, as the number of grams weight in a cubic foot of air or the number of grams in a cubic centimeter. We thus obtain the absolute humidity, which is defined as the mass of water vapour per unit volume of air.

1.5.1.2 Specific Humidity

Another measure of humidity, which has come into general use, especially in connection with upper-air observation is called specific humidity, defined as the weight of water vapour per unit weight of air (including the water vapour). Note that the absolute humidity is the relation of the weight of vapour to the volume occupied and specific humidity is the relation of weight of vapour to weight of air. Again, since the pressures exerted by gases are proportional to their masses, specific humidity may be obtained by dividing the partial pressure due to the water vapour by the total pressure of air.

When a quantity of air expands or is compressed, the total pressure and the vapour pressure change in the same ratio so that the value of this ratio remains the same. Hence, the specific humidity is constant under these conditions, it does not change unless water is added or removed [4].

1.5.1.3 Mixing Ratio

The mixing ratio is defined as the weight of water vapour per unit weight of completely dry air. It is the ratio of the water vapour to the remainder of the air. It thus differs from specific humidity only in using the pressure of dry air instead of the total pressure of the air.

1.5.1.4 Relative Humidity

Relative humidity is another way of expressing water-vapour content of the air. It may be defined as the ratio between the amounts of water vapour present to the amount required for saturation under fixed temperature and pressure conditions. Relative humidity is always expressed as a percentage or ratio. The amount of water vapour present in a unit volume of air is by definition the absolute humidity; hence the relative humidity equals the absolute humidity divided by what would be the absolute humidity if the air was saturated. Since vapour pressure, absolute humidity, specific humidity and mixing ratio are different ways of expressing the same thing, relative humidity may be expressed in each case as the ratio between the existing condition and the saturated condition [4].

1.5.2 Vapour Pressure and Saturated Vapour Pressure

When water vapour escapes into space and mixes with other gases of the air, it exerts a pressure in all directions as do the other gases. This is known in meteorology as vapour pressure of the air. It is independent of the pressure exerted by the other gases. The force exerted depends upon the concentration of the vapour, that is, upon the number of molecules per unit volume. It is commonly expressed in the same unit as the total air pressure, either in millibars or millimeter of mercury, referring to the length of the barometer column, which the partial pressure due to the water vapour would sustain.

Considering an open water surface, we find not only an escape of molecules from the liquid to the air but also some return of the gaseous molecules to the liquid. At first the number escaping will be greater than the number returning and we say that evaporation is occurring. But as the number of molecules of vapour in the air increases, there is an increase in the vapour pressure and in the number returning to the liquid until a point is reached when the number returning is just equal to

the number escaping. The net evaporation is then zero and the air is said to be saturated; that is, the space can hold no more water vapour under the existing conditions. If we now raise the temperature of the air, the tendency of the water vapour to return to a liquid state is decreased and we must add more vapour to keep the space saturated. At any given temperature, the saturated vapour pressure has a definite fixed value but the value changes rapidly with the change of temperature as may be seen in Fig. 1.5. For example: at -17.78°C the saturated vapour pressure is 0.09652 cm of mercury; at 10°C, saturated vapour pressure is 0.9144cm of mercury and at 37.78°C, saturated vapour pressure is 4.867 cm of mercury. These values have been determined by careful experiments [4].

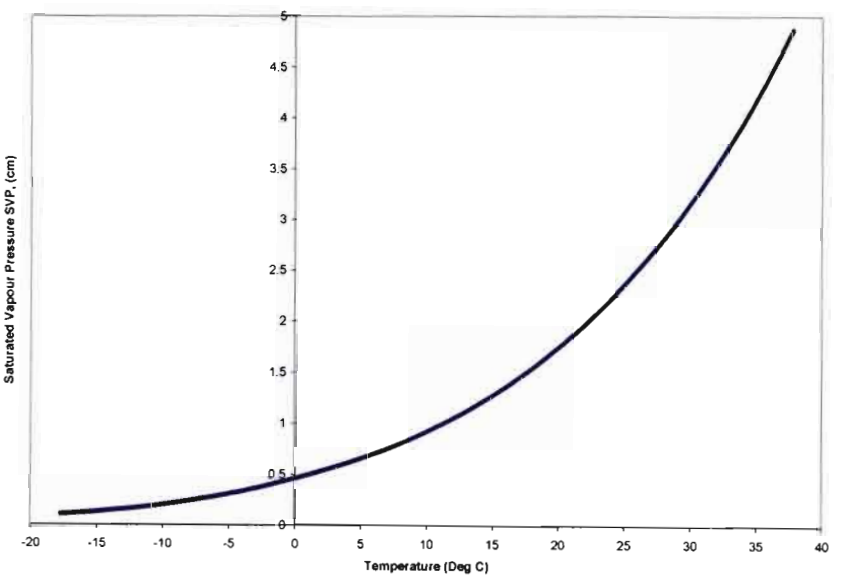

Fig. 1.5 Rapid Variation of Saturated Vapour Pressure with Temperature

1.6 Justification for the Dissertation

The median value of 4/3 normally used for effective earth radius factor (the k-factor) for communication planning is gradually becoming unacceptable due to the fact that true value of the k-factor in different parts of the world is found not to be 4/3 [5-6].

Hence there is a great need to come up with a reasonable estimate of the k-factor in different parts of the world especially in Africa. Limited available data for the African continent has been a major source of concern in communication system planning and design [7].

Over predictions of the refractivity variations can result in a costly over design of the system. On the other hand, under prediction results in the design of an unreliable system [8].

This study aims at determining the median and effective k values for both Botswana and Republic of South Africa and thus presents appropriate value of k-factor in this region so as to improve radio communication system design in the area.

Two height ranges of k values are used in the study, namely: 0-200m above ground level and 0-500m above ground level. The lower height range (0-200m) is used because there is not enough data in the 0-100m range which is normally the appropriate range for line-of-sight point-to-point radio link design. The other height range (0-500m) is chosen to account for link design used in media broadcasting such as TV broadcasting in the UHF and VHF band due to the taller towers employed in broadcasting.

1.7 Aims and Objective of Study

The objectives of this study are as follows:

(a) To calculate k-factor variation over several years within the height range 0-200m and 0-500m a.g.l.
(b) To compare k-factor variations in the months of February, May, August and November.
(c) To determine the median and effective k-factor variations.
(d) To formulate an analytical model for the k-factor probability density function.
(e) To compare the k-factor variations with those obtained elsewhere in the African region by Ajayi, Baker and Palmer, and Afullo et al among others, where possible.

CHAPTER TWO

2.1 Free Space Loss

In order to define the loss between the transmitting and receiving antenna separated by a particular distance we assume that the transmission medium between the transmitter and receiver is a vacuum. The antenna at each end of the link is assumed to be an isotropic one, so that we can say point A is an isotropic source[3]. Let the total power in watts radiated by the source be P_T. The envelope containing the radiation around the source can be considered to be an expanding sphere of radius r. The net power flow through the surface of a sphere at its center point is also P_T, hence, it follows that the power flow per unit area through any portion of the sphere's surface is given by [9]:

$$P_{av} = \frac{P_T}{4\pi r^2} \tag{2.1}$$

An isotropic antenna may serve either as a transmitting antenna or a receiving antenna. In the receive function, it absorbs power from the radiation field in which it is situated. Its effective aperture[4] determines the amount of power that the receiving antenna absorbs in relation to the RF power density of the field [9]. For an isotropic antenna, the effective area is $\lambda^2/4\pi$, where λ is the wavelength of the incident radiation field. From equation (2.1) it then follows that an isotropic antenna situated in a radiation field with a power density of P_{av} will deliver into its load a power P_R given by:

$$P_R = P_T\left(\frac{\lambda}{4\pi r}\right)^2 \tag{2.2}$$

Where r is the radius of the sphere. The transmission loss between transmit and receive antennas is defined as:

$$L_{dB} = 10\log_{10}\frac{P_T}{P_R} \tag{2.3}$$

Combining equations (2.2) and (2.3), the transmission loss becomes

$$L_{dB} = 21.98 + 20\log_{10}\left(\frac{r}{\lambda}\right) \tag{2.4}$$

---

[3] An isotropic source radiates uniformly in all directions (i.e. has a gain of 1 or 0 dB).
[4] Defined as the area of the incident wave front that has a power flux equal to the power dissipated in the load connected to the receive antenna output terminals.

Equation (2.4) can be re-expressed in a more useful form:

$$L_{dB} = 32.4 + 20\log r_{km} + 20\log f_{MHz} \tag{2.5}$$

Where r_{km} is the distance in kilometers between transmit and receive antennas and f_{MHz} is the frequency of the emitted radio field in megahertz. F is obtained as follows:

$$\lambda = \frac{c\,x\,10^{-6}}{f} \tag{2.6}$$

Where $c = 2.998x10^{8}\ m/\sec$, the velocity of light in free space.

2.2 Atmospheric Effects on Propagation

If a radio beam is propagated in free space where there is no atmosphere (by definition), the path followed by the beam is a straight line. The transmission loss in free space was derived in the previous section [9].

However, a radio ray propagated through the earth's atmosphere encounters variations in the atmospheric refractivity index along its trajectory that causes the ray path to become curved. Atmospheric gases will absorb and scatter the radio path energy, the amount of absorption and scattering being a function of frequency and altitude above sea level.

Absorption and scattering become serious contributions to transmission loss above 10 GHz (e.g. rain, water vapour, oxygen etc). Refractivity of the atmosphere will affect not only the curvature of the ray path (expressed by the k-factor) but will also give some insight into the fading phenomenon [9].

2.2.1 Refractive Effects on Curvature of Ray Beam

2.2.1.1 The k-factor

The k-factor is a scaling factor (actually assumed as a constant for a particular path) that helps quantify curvature of an emitted ray path. Common radio links, which are described as line-of-sight, incorrectly suggest that effective communications is limited by the optical horizon (i.e. k = 1) [9]. In most cases, radio links are not restricted to line-of-sight propagation. In fact communications beyond the optical horizon by some 15% (i.e. k = 1.33) can be achieved. Figure 2.1 shows this concept in a simplified fashion and Figure 2.2 shows the effect of various k-factors on the bending of the radio ray beam. This bending is due to angular refraction.

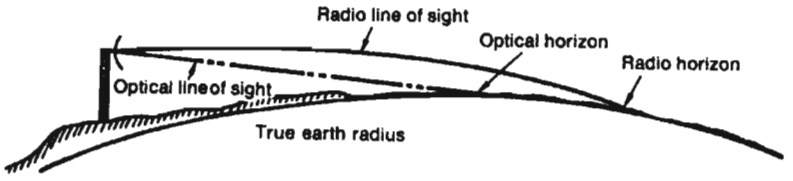

Fig. 2.1 Optical line-of-sight versus radio line-of-sight [9].

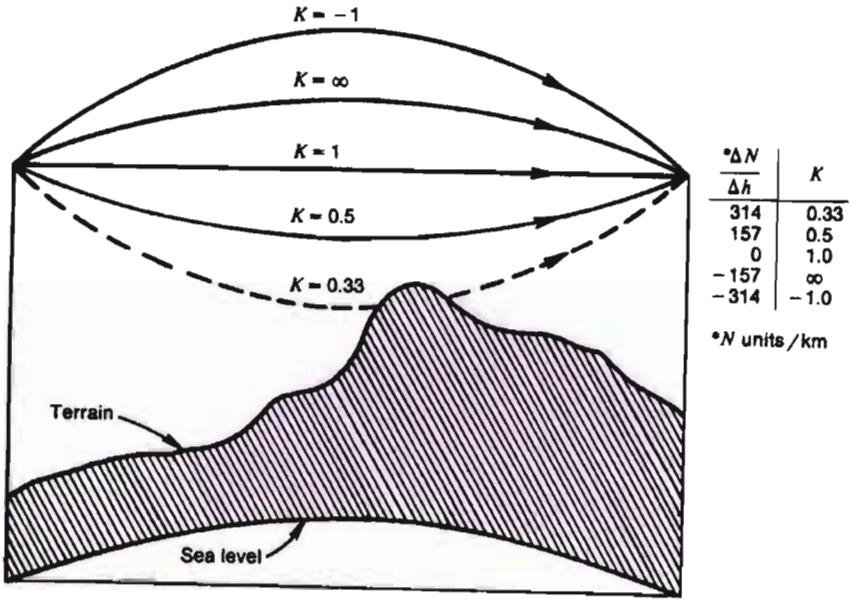

Fig. 2.2 Ray beam bending for various k-factors (linear refractivity gradients assumed) [9].

Angular refraction through the atmosphere occurs because radio waves travel with differing velocities in different parts of a medium of varying dielectric constant. In free space, the group velocity is maximum but in the nonionised atmosphere, where the dielectric constant is slightly greater due to the presence of gas and water molecules, the radio wave travels more slowly. In what radiometeorologists have defined as a standard atmosphere, the pressure, temperature and water vapour content (humidity) all decrease with increasing altitude [9]. The dielectric constant, being a single parameter combining the resultant effect of these three meteorological properties, also decreases with altitude. Hence electromagnetic waves travel faster in a medium of lower dielectric constant, the upper part of a wave front tends to travel with a greater velocity than the lower part causing a downward deflection of the beam. In a horizontally homogenous atmosphere where the vertical change of dielectric constant is gradual, the bending or refraction is continuous so that the ray is slowly bent away from the thinner density air toward the thicker, thus making the beam tend to follow the earth's curvature. This bending can be directly related to the radii of spheres. The first sphere is the earth itself (i.e. radius = 6370 km) and the second sphere is that formed by the curvature of the ray beam with its center coinciding with the center of the earth. The k-factor can now be defined as the ratio of the radius, a_e, of the ray beam curvature to the true radius of the earth, a, or

$$k = \frac{a_e}{a} \tag{2.7}$$

Where k is the effective earth radius factor and a_e is effective earth radius.

2.2.1.2 Refractivity and Refractivity Gradient

The radio refractive index is defined as the ratio of the velocity of propagation of a radio wave in free space to the velocity in a specified medium. At standard atmosphere conditions near the earth's surface, the radio refractive index (n) has a value of approximately 1.0003. However, in the design of radio systems, the use of a scaled-up unit is more desirable. This is called the refractivity (N), which is defined in the following relationships [9, 10]:

$$N = (n-1)10^6 \tag{2.8}$$

For the earth's atmosphere,

$$N = \frac{77.6}{T}\left[P + \frac{4810e}{T}\right] \tag{2.9}$$

Where

P = atmospheric pressure (hpa)

T = temperature (K)

e = water vapour pressure (hpa)

Of more direct interest to radio link design engineer are refractivity gradients. If we assume that the refractive index, n, of air varies linearly with the height h for the first few tenths of a kilometer above the earth's surface and does not vary in the horizontal direction, then we can restate the k-factor in terms of the gradient $\Delta n/\Delta h$ by:

$$\frac{a_e}{a} = k = \left[1 + a\frac{\Delta n}{\Delta h}\right]^{-1} \tag{2.10}$$

Where a = 6370 km and h is the height above earth's surface. Using equation (2.8) we have:

$$\frac{\Delta n}{\Delta h} = \frac{\Delta N}{\Delta h}(10^{-6}) \quad N - units/km \tag{2.11}$$

In Figure 2.2, there are several values of k and $\Delta N/\Delta h$ listed to the right. The Figure also illustrates sub-refractive conditions, $0 < k < 1.0$, where the refractive gradients are positive. The worst case in figure 2.2 is where the ray beam is interrupted by the surface, where k = 0.33, placing the receiving out of normal propagation range.

The more commonly encountered situation is where $\infty \geq k \geq 1.0$ or $-157 \leq \Delta N/\Delta h \leq 0$ [9]. In this case the ray has the same curvature as the earth and the ray path acts like straight line propagation over a flat earth.

It can be seen that the bending of a radio ray beam passing through the atmosphere is controlled by the gradient of refractive index. For most purposes, the horizontal gradient is so small that it can be neglected. The vertical change under standard atmospheric conditions is approximately - 40 *N*-units / km, which approximates the value at noon on a clear summer day at sea level in the temperate zone with a well mixed atmosphere. However, in the very lowest levels of the atmosphere, the vertical gradient may vary between extreme values as large as +500 to -1000 *N*- units/km over height intervals of several meters. The variance is a function of climate, season, time of day, and/or transient weather conditions. It is also affected by terrain, vegetation, radiational conditions and atmospheric stratification. The more extreme stratification tends to occur in layers less than 100 m in thickness and which at times extend over long distances. When averaged over 500 – 1000 m heights above ground, the radio refractivity gradient is likely to vary between 0 and -300 *N*-units/km. However, during a large portion of the year, the standard value of -40 *N*-units/km is more likely. Two refractivity parameters are commonly encountered when estimating radio propagation effects; these are surface refractivity N_s and surface refractivity reduced to sea level N_0 [9]. Dabideen [11] has calculated these values for Durban as: N_o = 349 N-units and $N_s = 349.\exp^{(-0.136hs)}$

2.3 Effective Earth Radius Factor Derivation

It is often convenient in solving propagation problems to consider the ray paths as straight lines instead of being curved as they actually are, and to compensate for the curvature by using a larger value for the "effective" radius of the earth [15]. The relations involved are shown in Fig. 2.3a and b. In Fig. 2.3a, the actual path is shown above an earth of radius a. In order for the straight-line path of Fig. 2.3b to be the equivalent of that shown in Fig.2.3a, it is necessary that the change in height dh be the same in the two cases for the same horizontal distance D [15]. In Fig. 2.3b,

$$dh = BO - AO = (ka + h)\left(\frac{1}{\cos\theta_e} - 1\right) \tag{2.12}$$

For small angles,

$$\frac{1}{\cos\theta_e} \approx \frac{1}{1-\frac{\theta_e^2}{2}} \approx 1+\frac{\theta_e^2}{2}$$

$$dh \approx \frac{ka\theta_e^2}{2}$$

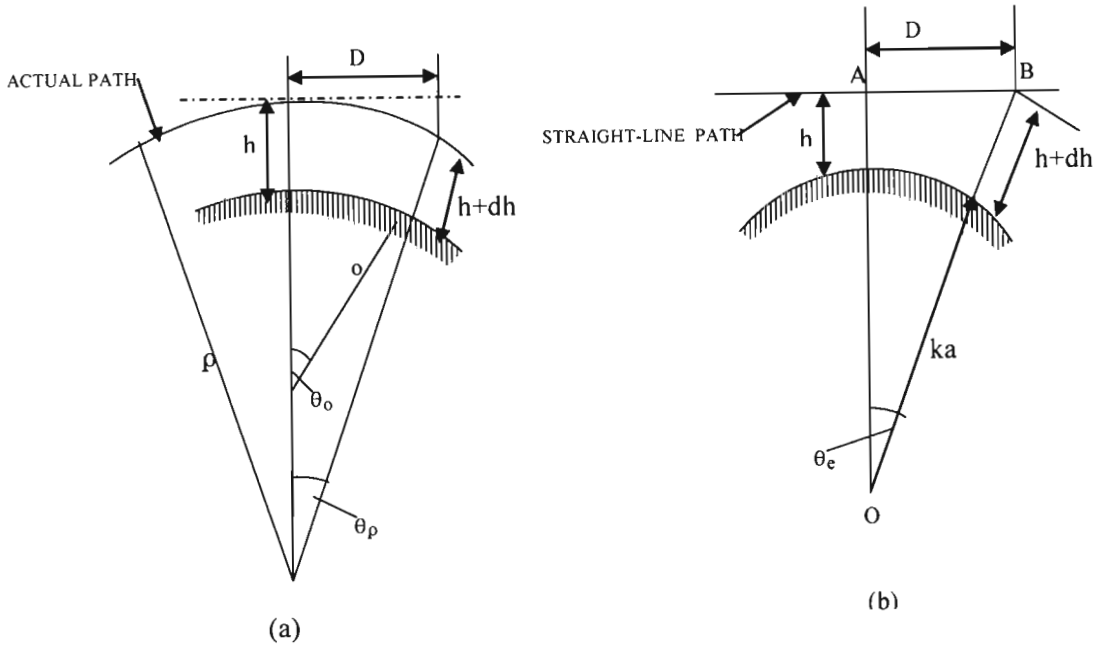

On the other hand, in Fig. 2.3a

$$dh = \frac{D^2}{2a} - \frac{D^2}{2\rho} \tag{2.14}$$

Combining equations (2.13) and (2.14) we therefore have:

$$\frac{1}{ka} = \frac{1}{a} - \frac{1}{\rho} \tag{2.15}$$

Hence

$$ka = a\left(\frac{1}{1-\frac{a}{\rho}}\right) \tag{2.16}$$

so that

$$k = \frac{1}{1-\frac{a}{\rho}} \tag{2.17}$$

where ka = effective radius of the earth

a = actual radius of the earth

k = effective earth radius factor (the k-factor)

ρ = radius of curvature of radio waves

The refraction of a radio wave in the atmosphere occurs because the dielectric constant and hence the refractive index of the atmosphere, varies with height above the earth. The dielectric constant of dry air is slightly greater than the value of unity that applies for vacuum and the presence of water vapour increases the dielectric constant still further. For this reason, the dielectric constant of the atmosphere is greater than unity near the earth's surface, but decreases to unity at great heights where the air density approaches zero. Although the dielectric constant and its variation with height are quantities that vary with the weather, the assumption is usually made that the variation of dielectric constant with height above the earth is uniform and an atmosphere that has the assumed condition is called a standard atmosphere. The justification for the use of a standard atmosphere in computation is that the results predicted on the basis of such an assumption agree fairly well with the results obtained in practice on the average [15].

In determining the k-factor, the relationship between the radius of curvature of the ray, ρ and the change of refractive index N, with height h, is very important. The relation between the radius of curvature of the path and the change of dielectric constant with height can be derived as follows.

If we let ρ be the radius of curvature of the path as stated earlier and v the velocity of propagation at a height h above the earth. Then from Figure 2.4

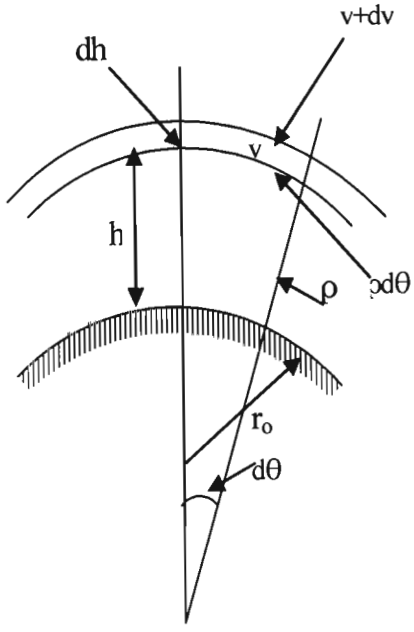

Fig. 2.4 Geometry of Earth Curvature [15]

$$\rho \, d\theta = v \, dt$$

or

$$\frac{d\theta}{dt} = \frac{v}{\rho} \tag{2.18}$$

Also

$$v = \frac{1}{\sqrt{\mu_v \varepsilon_r \varepsilon_v}} = k_1 \varepsilon_r^{-1/2} \tag{2.19}$$

At a height $h+dh = h + d\rho$, the velocity will be

$$(v+dv) = \frac{(\rho+dh)d\theta}{dt}$$

Therefore,

$$\frac{dv}{dh} = \frac{d\theta}{dt} = \frac{v}{\rho}$$

or

$$\rho = \frac{v}{dv/dh} = \frac{k_1 \varepsilon_r^{-1/2}}{-1/2 k_1 \varepsilon_r^{-3/2} \frac{d\varepsilon_r}{dh}} = -\frac{2\varepsilon_r}{d\varepsilon_r/dh}$$

Hence $\varepsilon_r \approx 1$

$$\rho = -\frac{2\varepsilon_r}{d\varepsilon_r/dh} \tag{2.20}$$

Substituting equation (2.20) into (2.17) we then have

$$k = \frac{1}{1 - a/\rho} = \frac{1}{1 + a\frac{d\varepsilon_r/dh}{2}} \tag{2.21}$$

Where h is the height above ground level and ε_r the permittivity of the troposphere.

The radius of curvature of the path ρ, being a function of the change of dielectric constant with height h, varies from hour to hour, day to day and season to season. That is why the ITU-R gives plots of refractivity and refractivity gradient for the months of February, May, August and November. In Botswana, these reference months correspond to the following seasons: Peak rainy summer (February); transition to winter (May); dry winter (August) and transition to summer (November).

The refractive index, n is related to ε_r and refractivity N as follows;

$$n = \sqrt{\varepsilon_r}; \quad N = (n-1)10^6 \tag{2.22}$$

We can derive k in terms of refractive index, n, and refractivity, N, as follows:

The refractive index of the troposphere, n, varies with height, hence the relation between radius of curvature of the ray and refractive gradient is given as:

$$\frac{1}{\rho} = \frac{-dn}{dh} \tag{2.23}$$

Where

n = refractive index of the atmosphere

h and ρ maintain their usual definition

Substituting equation (2.23) into (2.15) we have

$$\frac{1}{ka} = \frac{1}{a} + \frac{dn}{dh}$$

so that

$$ka = a\left(\frac{1}{1+a\frac{dn}{dh}}\right)$$

and

$$k = \left(\frac{1}{1+a\frac{dn}{dh}}\right) \tag{2.24}$$

Where a = Earth's Radius (6.37×10^3 km)

Where k = effective earth radius factor (k-factor)

But

$$N = (n-1)10^6 \quad N\text{-unit}$$

$$\therefore k = \frac{1}{1+a\frac{dN}{dh}10^{-6}} \tag{2.25}$$

But

$$a = 6.37x103km = 40{,}000/2\pi$$

Substituting the value of a, into equation (2.25) we have:

$$k = \frac{1}{1+\frac{dN}{dh}x6.37x10^{3}x10^{-6}} = \frac{1}{1+\frac{dN}{dh}x\,6.37\,x\,10^{-3}} = \frac{1}{1+\frac{dN}{dh}x\,0.00637} \qquad (2.26)$$

But $$0.00637 \approx \frac{1}{50\pi}$$

Hence

$$k = \frac{1}{1+\frac{dN}{dh}\Big/50\pi} \qquad (2.27)$$

2.4 Path Profiles

A path profile is a graphical representation of a path between two adjacent radiolink sites in two dimensions. From the path profile, tower heights are derived and subsequently these heights can be adjusted (on paper) so that the ray beam reflection point will avoid reflective surfaces. The profile essentially ensures that the proper clearances of path obstructions are achieved. There are three recognised methods to draw a path profile: Fully linear method, earth method and curvature method.

2.4.1 Fully Linear Method

Common linear graph paper is used where a straight line is drawn from the transmitter site to receiver site giving tangential clearance of equivalent obstacle heights. A straight line is also drawn from the receiver site to the transmitter site. The bending of the radio beam is represented by adjustment of each obstacle height by equivalent earth bulge using equation (2.28).

$$h = \frac{d_1 d_2}{12.75k} \qquad (2.28)$$

Where h is the change in vertical distance in meters from a horizontal reference line, d_1 is the distance in kilometer from one end of the path to obstacle height in question, and d_2 is the distance from other end of path to the same obstacle. k is the selected k-factor [9].

2.4.2 4/3 Earth Method

The 4/3 earth paper is required for this method. In this case, true values of obstacle height may be used. An example of a profile using 4/3 graph paper is shown in Figure 2.5. This method keeps the value of k fixed at 4/3.

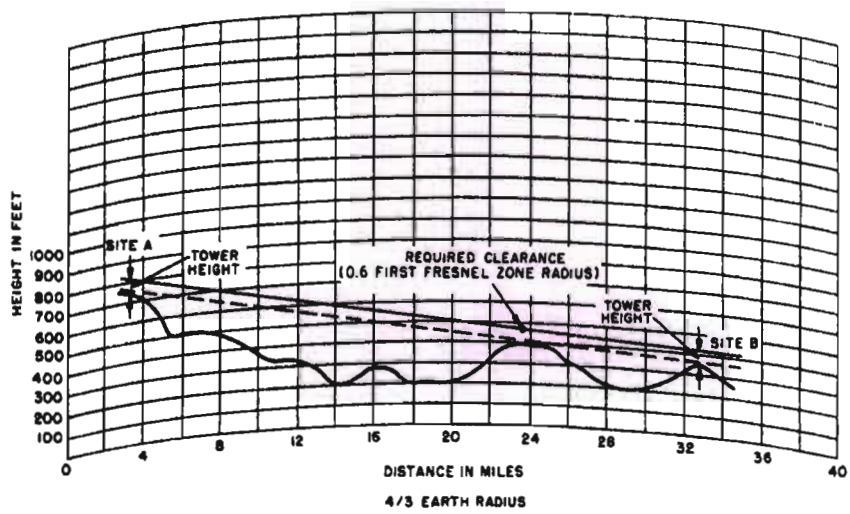

Fig. 2.5 Illustration of path profile method 2 using 4/3 earth graph paper [9]

2.4.3 Curvature Method

Linear graph paper is used in this method. True values of obstacle heights are employed from a reference line or mean sea level (MSL) and a curve is drawn from transmitter site (arbitrarily one end) to the receiver site and vice versa. The curved line has a curvature ka, where k is the applicable k-factor and a is the geometric radius of the earth or 6370 km assuming the earth is a perfect sphere.

2.5 Diffraction Effects

2.5.1 The Fresnel Ellipsoids

Diffraction of radio wave fronts occurs when the wave front encounters an obstacle that is large when compared to the wavelength of the ray. Below about 1000 MHz there is diffraction or bending from an obstacle with increasing attenuation as a function of obstruction height. Above about 1000 MHz, with increasing obstruction of an obstacle, the attenuation increases even more rapidly such that the path may become unstable by normal transmission means than of lower frequencies. The actual amount of obstruction loss is dependent on the area of the beam obstructed in relation to the total frontal area of the energy propagated and to the diffraction properties of the obstruction [9].

Under normal transmission conditions (i.e. non diffraction), the objective for the system designer is to provide sufficient clearance of the obstacle without appreciable transmission loss due to the obstacle. To calculate the necessary clearance wave physics Huygen's principle and the theory developed by Fresnel are employed. When dealing with obstacle diffraction, we assume that the space volume is small enough that gradient effects can be neglected so that the diffraction discussion can proceed as though in an homogeneous medium.

Consider Figure 2.6, the Huygens–Fresnel wave theory states that the electromagnetic field at point S_2 is due to the summation of the fields caused by radiation from small incremental areas over a closed surface about a point S_1, provided that S_1 is the only source of radiation. The field at a constant distance r_1 from S_1, which is a spherical source, has the same phase over the entire surface hence the electromagnetic wave travels at a constant phase velocity in all directions in free space. The constant phase surface is called a wave front. If the distances r_2 from the various points on the wave front to S_2 are considered, the contributions to the field at S_2 make up of components that add vectorially in accordance with their relative phase differences. Where the various values of r_2 differ by half-wavelength ($\lambda/2$), the strongest cancellation occurs. Fresnel zones distinguish between the areas on a closed surface about S_1 whose components add in phase.

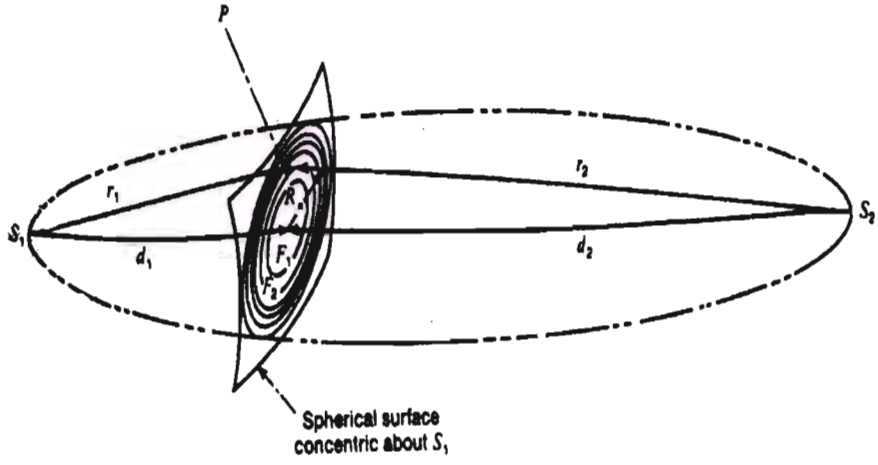

Fig. 2.6 Fresnel Zone Geometry [9]

Let us consider a moving point P_1 in the region about the terminal antenna locations S_1 and S_2 such that the sum of the distances r_1 and r_2 from the antennas to P is constant. Such a point, then, will generate an ellipsoid with S_1 and S_2 as its foci. We now can define a set of concentric ellipsoidal shells so that the sum of the distances r_1 and r_2 differs by multiples of half-wavelength ($\lambda/2$). The intersection of these ellipsoids defines Fresnel zones on the surface as shown in Figure 2.6. Thus, on the surface of the wave front, a first Fresnel zone F_1 is defined as bounded by the intersection with the sum of the straight line segments r_1 and r_2 equal to the distance d plus one-half wavelength ($\lambda/2$). The second Fresnel is defined as the region where $r_1 + r_2$ is greater than $d + \lambda/2$ and less than $d + 2(\lambda/2)$. Thus the general case may now be defined where F_n is the region where $r_1 + r_2$ is greater than $d + (n-1)\lambda/2$ but less than $d + n\lambda/2$. Field components from even Fresnel zones tend to cancel those from odd zones since the second, third, fourth, and fifth zones (etc.) are approximately of equal area.

Fresnel zone application to path obstacles may only be used in the far field. The minimum distance d_F where the Fresnel zone is applicable may be roughly determined by $d_F > 2D^2/\lambda$, where D is the antenna aperture measured in the same unit as λ. To calculate the radius of the n^{th} Fresnel zone r_n on a surface perpendicular to the propagation path, the following equation provides a good approximation:

$$r_n = \sqrt{n\lambda\left(\frac{d_1 d_2}{d_1 + d_2}\right)} \tag{2.29a}$$

or

$$r_n = 17.3\sqrt{\frac{n}{f_{GHz}}\left(\frac{d_1 d_2}{d_1 + d_2}\right)} \tag{2.29b}$$

Where d_1 is the distance to the near end antenna and d_2 is the distance to the far end antenna from the obstacle, and in equation (2.29b) all distances are in kilometers, the frequency of the emitted signal is in gigahertz and r_n is in meters. Conventionally we require 0.6 Fresnel zone clearance of the beam edge (3-dB point) due to obstacle in the path. Providing 0.6 Fresnel zone clearance usually is sufficient to ensure that attenuation due to obstacle in or near the ray beam path is negligible [9].

2.5.2 Link Budget and Link Reliability

For a radio line of sight link, there are losses associated with the radio wave signal as it travels from the transmitter to the receiver. The total path loss associated with the transmitted signal is given by [16]:

$$L_{tot} = L_{fs} + K_l + L_o + L_r + L_v + L_{fad} \tag{2.30}$$

Where:

L_{fs} = *Free Space Loss*

K_l = *Correction factor of free – space loss (medianloss) = −16dB for Raleigh – faded path*

L_o = *oxygen loss* ($\approx 50\ GHz$)

L_r = *rain loss depends, on rain rate*

L_v = *Water Vapour Loss* ($> 10\ GHz$)

L_{fad} = *Fade margin, due to multipath effects.*

If link is not line of sight (NLOS) however, then we also include a diffraction loss, L_d. A design value of k which results in less than 60% clearance of first Fresnel zone results in some non-zero diffraction loss. If $k = k_1$ is used in the design, then earth bulge, b_1, is experienced at point of maximum obstruction. The antenna designed is such that at maximum obstruction point, 60% of first Fresnel zone radius is achieved. However if the actual value of k is k_2, the earth bulge is b_2.

Then there is obstruction of the first Fresnel zone if $b_2 > b_1$ (that is, more than 60% r_1 is obstructed).

Fresnel zones explain the concept of diffraction loss as a function of path clearance around an obstruction. The derivation of Fresnel zones radius was detailed in the last section. It should be noted that the Fresnel zones are elliptical in shape with the transmitter and receiver at their foci [17].

2.5.3 Knife – Edge Diffraction Loss

Assume a knife edge obstacle made up by a perfect conductor half plane, normal to the direction of propagation. In this ideal case the obstacle may be defined by a single non-dimensional parameter v given by [18]:

$$v = \pm h \sqrt{\frac{2d}{\lambda d_1 d_2}} \tag{2.31}$$

Where:

h is the obstacle height above (plus sign) or below (minus sign) the direct ray between the transmitter and receiver antennas (see Fig.2.7) ; d is the distance between the antennas; d_1 and d_2 are the distances between the obstacle and each of the antennas; λ is the wavelength corresponding to the operating frequency f. Parameter v may also be expressed as a function of the radius of the first Fresnel ellipsoid r_{1e} at the obstacle. From equations (2.29a) and (2.31) we get [18]

$$v = \pm h \frac{\sqrt{2}}{r_{1e}} \tag{2.32}$$

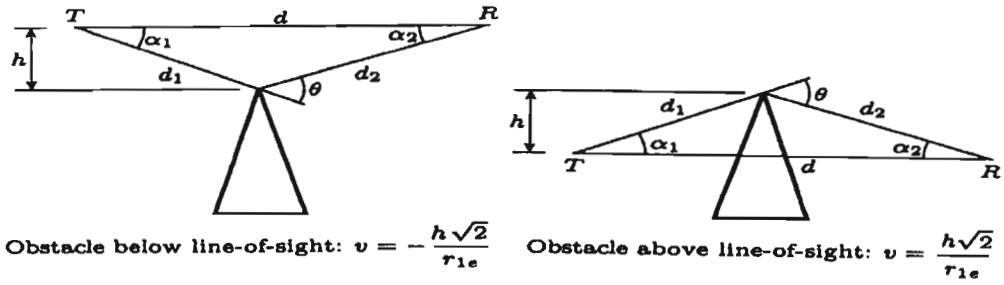

Fig. 2.7 Definition of v for obstacles above and below line-of-sight [18]

Estimating the signal attenuation caused by diffraction of radio waves over hills and buildings is essential in predicting the signal strength in a given service area. The electric field strength E_d of a knife-edge diffraction wave is given by [17]:

$$\frac{E_d}{E_O} = F(v) = \frac{(1+j)}{2}\int_{v}^{\infty} \exp((-j\pi t^2)/2)\,dt \qquad (2.33)$$

Where E_o is the free space field strength in the absence of both the ground and the knife edge, and $F(v)$ is the complex Fresnel integral. The Fresnel integral, $F(v)$, is a function of the Fresnel-Kirchoff diffraction parameter v.

The diffraction gain due to the presence of a knife-edge as compared to the free space electric field is given by [17]:

$$G_d(dB) = 20\log|F(v)| \qquad (2.34)$$

In practice, graphical or numerical solutions are relied upon to compute diffraction given. Rappaport [17] approximate equation (2.34) as follows:

$$\left.\begin{array}{cc} G_d(dB) & v \\ 0 & v \le -1 \\ 20\log(0.5-0.62v) & -1 \le v \le 0 \\ 20\log(0.5\exp(-0.95v) & 0 \le v \le 1 \\ 20\log\left(0.4-\sqrt{0.1184-(0.38-0.1v)^2}\right) & 1 \le v \le 2.4 \\ 20\log\left(\frac{0.225}{v}\right) & v > 2.4 \end{array}\right\} \qquad (2.35)$$

Using equation (2.35) Knife-edge diffraction gain can be plotted for different value of Fresnel parameter v as shown in figure 2.8.

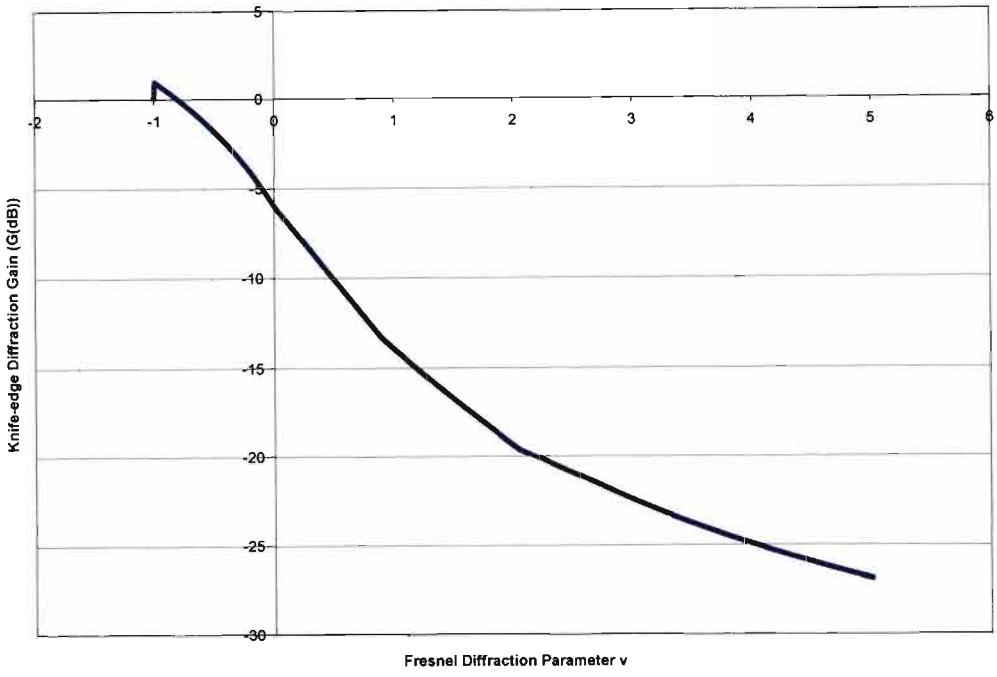

Fig. 2.8 Knife-edge diffraction gain as a function of Fresnel diffraction parameter v

2.6 The Proposed Model for the k-factor Distribution

A model is proposed for the probability density function (pdf) of the effective earth radius factor in Botswana and Durban, after an analysis of the three years and ten months data respectively as a means of predicting the k-factor variation [8]. This model is based on the radiosonde measurement data obtained in [11] and [19]. The model is based on the minimum sum of square error between g(k), the measured pdf and f(k), the analytical estimation of the pdf. We use f(k) to determine k_e[5] for the height ranges 0-500m and 0-200m above ground level. The procedure embarked upon in the model formulation is explained in this section.

[5] Effective k, value of k exceeded 99.9% of the time.

2.6.1 Modeling of the k-Factor

From the results in [19], it was concluded that the distribution of k is bell-shaped, centered almost symmetrically about a mean value, μ_k. This can also be seen in the later chapter, where the distribution of k-factor exhibits the stated bell shape. Therefore the following pdf, f (k) was proposed:

$$f(k) = Ae^{-\alpha(k-\mu_k)^2} \tag{2.36}$$

The parameter A is the value of f(k) at the mean, μ_k while the parameter α determines the girth of f(k). The task is therefore to determine A, μ_k, and α. The following conditions have to be satisfied:

$$\int_{-\infty}^{\infty} f(k)dk = \int_{-\infty}^{\infty} Ae^{-\alpha(k-\mu_k)^2} dk = 1 \tag{2.37}$$

$$E\{k\} = \int_{-\infty}^{\infty} kAe^{-\alpha(k-\mu_k)^2} dk = \mu_k \tag{2.38}$$

In order to ascertain f(k) as the "best" approximation for g(k), we need to optimize a cost function related to the error, ε (k). The cost function we choose is the integral of the square error (ISE).

$$\begin{aligned} \varepsilon(k) &= [f(k) - g(k)] \\ ISE &= \int_{-\infty}^{\infty} [f(k) - g(k)]^2 dk \end{aligned} \tag{2.39}$$

Thus the minimum value of the square of the error in (2.39) will determine the optimum choice of f (k) parameters A, μ_k, and α. An algorithm was therefore developed for determination of the parameters A, μ_k, and α, which gave the minimum error in (2.39). The algorithm is as follows:

a) As a first estimate, choose μ_k from the plot of g(k).
b) Next, choose A such that:

$$A = g(k)\big|_{k=\mu_k} \tag{2.40}$$

c) Now determine the corresponding α to fulfill the conditions (2.37) and (2.38).
d) Calculate the ISE from (2.39).

e) Then, with mean constant at μ_k, vary A and α to satisfy conditions (2.37) and (2.38). For each combination (A, α), determine the ISE.

f) From the procedure in (e) above, identify the combination (μ_k, A_m, α_m) such that ISE is a minimum.

g) Finally, with (A_m, α_m) fixed, vary the mean, μ_k until the lowest ISE is achieved. This gives the optimum combination (A_m, α_m, μ_{km}).

h) Then the best estimate for the pdf becomes:

$$f(k) = A_m e^{-\alpha_m (k-\mu_{km})^2} \tag{2.41}$$

The assumption here is that there exist a global minimum, hence this is the limitation of the algorithm.

Using the foregoing procedure, the optimum f(k) was obtained (which gives the best estimate of f*(k)) for the months of February, May, August, and November. The overall f (k) for the whole year was also determined. Initially, the results were restricted to data within the height range 0-500 m a.g.l. Thereafter, height range 0-200 m a.g.l. was considered.

Initially, in order to satisfy criteria given in (2.37) and (2.38) A and α were determined to have the following relationship:

$$\alpha = \pi A^2 \Rightarrow A = \sqrt{\frac{\alpha}{\pi}} \tag{2.42}$$

This is the standard relationship for a normal distribution; the plot of equation (2.37) that satisfies the given criteria (2.37) and (2.38) is shown in Fig. 2.9.

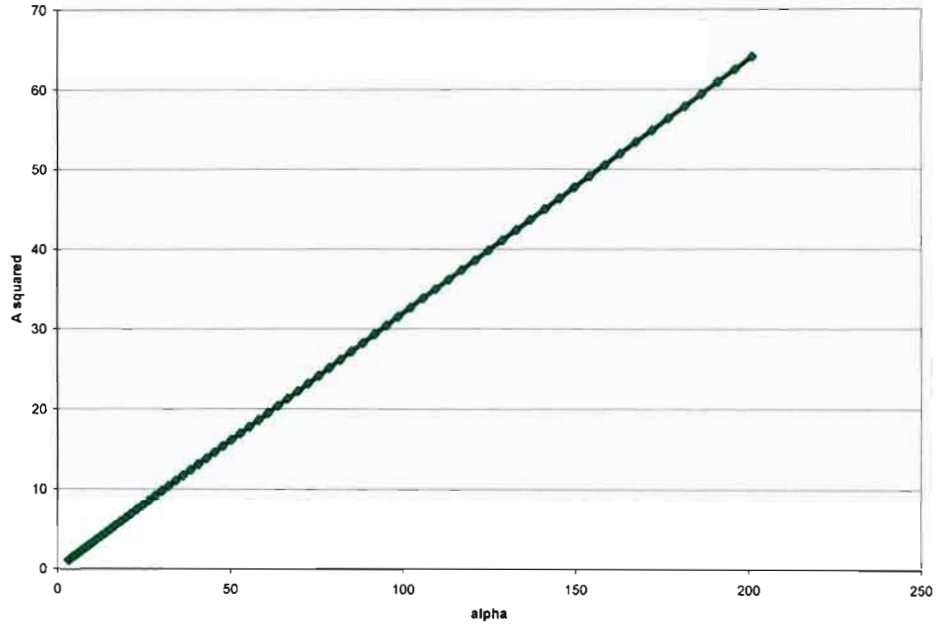

Fig. 2.9 Variation of alpha versus A squared (To satisfy equations (2.37) and (2.38))

CHAPTER THREE

3.1 Global Studies on Radioclimatological Modeling

Olsen [7,20] provides a summary of global work on radioclimatological modeling. In his submission, extensive use of digital microwave radio links in the communications networks of various countries over the last fifteen years has resulted in a renewed interest in methods of predicting the effects of multipath fading [7,20]. Although emphasis has shifted to studies of wide-band effects such as distortion, there has remained a strong interest in the development of accurate methods for predicting the multipath fading distortion in narrow frequency band (sometimes referred to as "single-frequency" methods) under varying climatic conditions. In fact, narrow-band prediction techniques are necessary elements of virtually all techniques for predicting the outage of digital links. As distortion has been reduced through the use of improved equalization techniques, this narrow-band element in outage prediction has been gaining importance. Currently, the narrow-band fading distribution is the most widely available multipath fading statistic and, therefore, the one most suitably characterised in terms of climatic conditions [7,20].

Techniques for predicting the deep-fading range of the multipath fading distribution for the average worst month have been available for many years [20]. Most of these have been based on empirical fits of Rayleigh-type distribution (i.e. with slopes of 10 dB/decade) to the fading data for individual countries. The best known techniques in this category are those of Morita for Japan, Bernett and Vigants for United States, Person and Doble for the United Kingdom, Nadenenko for the former Soviet Union and that of the International Radio Consultative Committee (CCIR) for "Northwest" Europe. The techniques of Boithias, although designed for shallow as well as deep fading and conforming to a Rice-Nakagami distribution rather than Rayleigh-type distributions was also fitted to fading data for "Northwest" Europe. Although these techniques have been used to varying extent in other parts of the world, link designers in other countries have been faced with the difficulty of choosing among techniques sometimes giving vastly varying different results for the same apparent climatic region.

To overcome this problem in 1988, the Study Group 5 of the CCIR (now ITU-R) adopted two "worldwide techniques for predicting the deep-fading range of the multipath fading distribution [7,20]. The first method did not require detail path profile information and was specified as best

suited for preliminary planning or licensing purposes. It needed only path length, frequency and path inclination as input variables. The second method however did require the path profile in order to obtain an additional link variable (the "average" grazing angle of the wave specularly reflected from the ground), and was specified as more appropriate for link design.

The ITU-R data base assembled by different authors contained data for 246 links in 23 countries at frequencies between 450 MHz and 37 GHz in regions from mountainous to over water. Detailed results were presented on the basis of countries, regions within countries and terrain-climatic regions. The error statistics demonstrate the considerable improvement of the revised geoclimatic factor model over the original model. The ability of the revised model to follow the large-scale variability over a large area of the world is evidenced by the relatively small mean errors from country to country and from region to region within the countries. At the same time they demonstrate that no significant overall advantage is gained by employing the second method (with its additional variable obtained from a calculation of the path profile) over the first method. Overall mean and standard deviation or error for revised first and second methods on overland paths are 1.0 and 6.2 dB, and 0.4 and 6.1 dB respectively. Nevertheless, the slightly better ability of the second method to follow large-scale geoclimatic variations from one region to another (4.1 and 4.5 dB for the standard deviation of regional mean errors) suggests the possibility of future improvements using one or more path-profile predictor variables.

On the basis of a detailed analysis of the various sources of error, it was shown that the largest contribution to the overall standard deviation of error is that due to the geoclimatic factor model. The corresponding contributions to the overall standard deviation of error on overland path was estimated as 4.8 dB for the first method. Whereas, that due to the link-variable model (the next most important) was estimated to be at most 3.4 dB. Since these errors must be combined in terms of the corresponding variances, further work to improve the geoclimatic factor model is clearly very important.

New multipath model was proposed in [21] and the model was based on Rayleigh distributed reflections and refractions. It includes consideration of reflected /refracted signal amplitude, delay and time variability. This multipath model is able to describe all the effects observed on paths that are dominated by refractive and reflective mechanisms. Key to this new understanding of microwave radio paths is the understanding of the role of ducts which occur in the lower troposphere. The k-factor appears to be linearly constant around 4/3 for the majority of the lower

troposphere but can vary substantially in the vicinity of a duct. In order to implement this model, accurate data is required about the characteristics of ducts that are likely to cause reflections/refractions on line-of-sight microwave radio paths. The information required includes [21]:

1. The occurrence probability of the various types of ducts.
2. The height of the duct and its height variability
3. The strength of the duct and dN/dh with 0.5m resolution
4. The radiometeorological characteristics of the duct so that a radio system designer can determine which ducts are important in design

The measurements carried out in [21] reveal a wide variety of different types of meteorological situations which are capable of forming ducts that will reflect or refract microwave radio signals resulting in fading. More radio meteorological information on ducts is however required to enable the potential of this model to be fully realised.

Statistics of super-refraction and ducting are used to characterise the effects of climate on the propagation of radio waves. Comparisons of refractivity statistics derived from low and high resolution data and reasons for any differences are examined in [22]. The enhanced vertical resolution of the raw data enables the identification of strong thin elevated layers of ducting, which may not be represented in the low resolution data. While this fine structure may have little significance from a meteorological point of view, the effect on propagation could well be significant and this is investigated through the use of parabolic equation modeling. Statistics of these layers are presented in [22].

3.2 African Scenario

Ajayi et al report on radioclimatological measurements carried out at three locations in Africa, namely: Douala (Cameroun), Ile-Ife (Nigeria) and Nairobi (Kenya) under the joint African radiometric Measurement Campaign in the latter part of 1980s [23]. In their analysis, the specific attenuation due to rain can be obtained either theoretically or practically by using empirical scaling procedure between specific attenuation and rain rate [23]. The effective propagation constant for a linearly polarized wave can be computed directly for spheroidal raindrops using the relation:

$$k_{V,H} = \frac{2\pi}{k_0} \int f_{V,H}(k_1, k_1) N(D) dD \qquad (3.1)$$

Where $f_{V,H}(k_1 k_1)$ represents the vector scattering amplitude function in the forward direction, k_0 is the free space wave number, and $N(D)dD$ defines the number of raindrops per unit volume and per diameter interval. Ajewole et al (1999) [25] computed the complex effective propagation constant using the lognormal drop size distributions obtained for four different types of tropical rainfall by Adimula and Ajayi, 1996. The specific attenuation has been calculated from the imaginary part of the effective propagation constant in the rain medium for a path length (L) taken as 1 km using the following relation [23]:

$$A_{V,H} = 8.686\ x\ \mathrm{Im}(K_{V,H} L)\ (dB/km) \tag{3.2}$$

Where

$A_{V,H}$ = *Specific attenuation*
L = *Path length in km*

It is observed that for frequencies in the K_u band ~ 12.56 GHz and higher frequencies, attenuation due to rain becomes so high that complete outage of signals could occur unless special provisions are made to combat this attenuation.

The long-term statistics of the slant-path rain attenuation at a given location for frequencies up to 55 GHz is discussed as a case study. The prediction system has undergone several modifications over the years and one of the problems has to do with the scanty measurements in the tropical regions including Africa. It is observed that the prediction technique is now more complex than it used to be in the past. The estimation requires the following parameters:

$R_{0.01}$: point rainfall rate for the location for 0.01% of an average year (mm/h)
h_s: height above mean sea level of the earth station (km)
θ: elevation angle (degrees)
φ: latitude of the earth station (degrees)
f: frequency (GHz)
R_e: effective radius of the Earth (8500 km)

3.3 Southern Africa

Communication engineers in South Africa have commonly used k = 4/3 when planning radio communication systems. This approach, as already discussed is an oversimplification of what happens in the real word. Hence, this simplistic approach can lead to inadequate designs requiring costly reverse engineering. That is why Baker and Palmer [12] proposed a model for k-factor determination that addresses this oversimplification. They use available South African and Namibian data to test their model [12]. They use regression analysis method with data obtained from eight different stations in South Africa, namely; Alexander Bay, Cape Town, Durban, Upington, Port Elizabeth, Bloemfontein, Pretoria and Windhoek. In their analysis, they report using equations (2.27) that k-factor comprises both a "dry" term and a "wet" term. It was then proposed that the cumulative distribution describing the probability that the k-factor exceeds a particular value, say k' could be approximated by

$$\psi(k \geq k') = \exp\left\{-(k-1)^2/(2\sigma^2)\right\} \tag{3.3}$$

where σ^2 is the variance of k. Expression (3.3) give rise to a formula, which in turn could be used in a regression analysis, namely

$$\sqrt{\ln(1/\psi)} = \frac{(k-1)}{\sqrt{2}\sigma} + c \tag{3.4}$$

where c is a constant.

3.3.1 The "Dry-Wet" Model

The observed cumulative data seemed to be the result of two separate cumulative distributions, assumed to be independent. It was therefore proposed to represent the effective cumulative distribution as the product of two statistically independent cumulative distributions so that [12]

$$\psi_{eff}(k \geq k') = \psi_{dry} \times \psi_{wet} \tag{3.5}$$

Where

$$\psi_{dry} = \exp\left\{-(k-1)^2/\left(2\sigma_{dry}^2\right)\right\} \tag{3.6}$$

and

$$\psi_{wet} = \exp\left\{-(k-k_{ref})^2/\left(2\sigma_{wet}^2\right)\right\} \tag{3.7}$$

The reference value of k, k_{ref}, was to be determined during regression analysis of data. Equations (3.5), (3.6) and (3.7) were manipulated to develop a regression formula of the form:

$$\ln\sqrt{1/\psi} = c + m_1 k + m_2 Abs(k-k_{ref}) \tag{3.8}$$

It was found that this form compressed the resultant data for values of k close to unity too much, resulting in significant loss of sensitivity of the method for these values. It was therefore decided to use the same basic form as in equation (3.4), namely

$$\sqrt{\ln(1/\psi)} = c + m_1 k + m_2 Abs(k-k_{ref}) \tag{3.9}$$

The results thus obtained from the regression analysis were statistically only marginally worse than those from equation (3.8), but did retain the desired sensitivity for values of the k-factor close to unity. They report that on the basis of the results obtained, it has been possible to generate contour maps South Africa showing the expected k-factor for a given cumulative distribution. Also, they note in[13] that the basic model reported appears to account manly for the "dry" component of the refractive index, as reflected in the k-factor. They conclude from this research that the model will assist in predicting large values of k-factor that may only be exceeded rarely in the inland summer rainfall area [13].

Their work has been further extended to incorporate thirty stations instead of the previous eight [5]. In this new study, they use ground base data to test their model and were able to show that their results agree with the earlier work when they used radiosonde data except for the station at Alexander Bay.

In an accompanied paper they use the model developed in the first paper to predict the cumulative earth radius factor (the k-factor) for different months as a function of height [6]. Comparisons between predicted and observed results were presented in [6]. It can be observed from [6] that the k-factor varies between 1.12 and 1.21 for all months at occurrence probability of 99.99% for the

observed value in Pretoria, while it varies between 1.14 and 1.20 for all months at occurrence probability of 99.99% for the predicted values in the same location [6]. A median value of k = 1.5 was observed for Durban at height 8m a.g.l. while the predicted mean value is k = 1.46 a.g.l. at the same height in Durban [6].

A thorough study on refractivity variation based radiosonde measurements carried out in Maun, northern Botswana was done in [1]. From the measurements it was established that the lowest surface refractivity occurs in August while the highest occurs in February for an average afternoon in Botswana. But for the average post-midnight, surface refractivity has its lowest value in August and highest value in November. As far as refractivity gradients are concerned, it was observed that afternoon ducts tend to occur in the month of February, while post-midnight ducts occur in the month of November.

Seasonal variation of radio refractivity in Botswana is studied in [2], the data used for the study covers a 12 calendar months. In the analysis, the refractivity gradient is restricted to a region within 200m a.g.l. It is observed that while the daytime average refractivity gradient averages about -16 N-units /km, the night-time average is about -58 N-untis/km. It is also observed that within this height range, ducting is quite prevalent during the October-December quarter, while it is less of a problem during the other quarters. The refractivity gradient dN/dh for four quarters were presented in the study, the four quarters are: first quarter (January, February and March), second quarter (April, May and June), third quarter(July, August and September) and the fourth quarter (October, November and December).

The first and fourth quarters fall roughly within the summer season, while the second and third quarters roughly fall within the winter season. The following observations were made from the study; during the day, the average refractivity gradient varies between -12 and -20 for all the four seasons. The highest values of dN/dh were also observed, high values near or exceeding -40 N-units/km ($k \leq 0.8$) are observed at least once in all the four seasons, refractivity values corresponding to dN/dh > 15 ($k < 0.91$) occur for about 10% of the days (or time) for each season.

The nights are observed to be super-refractive as expected, the seasonal averages for the nights are fairly close: -60 N-units/km for the second and third quarters, and -55 N-units/km for the fourth quarter. Lowest values of dN/dh exhibit a seasonal variation, during the second quarter

(corresponding to start of winter), the lowest value recorded within the 7 measurement days is -120 N-units/km. During the third quarter (peak and end of winter), two values below -140 N-units/km are recorded, with another three values below -110 N-units/km. However, still no ducting takes place yet. During the fourth quarter (start and mid-summer), five ducts are recorded, four of which have dN/dh falling below -200 N-units/km, with another five values below -100 N-units/km.

Form the dN/dh values of ITU plots, the percentage of the time when dN/dh< -100 N-units/km for the Southern Africa region covering Botswana are: 5-10% for February; 2-5% for May; 2-5% for August and 0-20% for November. From the figures presented in [2] the corresponding values (using the combined low night and low day data) are 4% for second quarter; 16% for third quarter; and 13% for the fourth quarter. These are thus found to be in agreement with the ITU plots.

Estimates of refractivity gradient and k-factor ranges are also done by the same authors for Botswana in [19]. From this study they report that the median value of dN/dh is -20N-units/km, with a high occurrence rate during the winter, and a lower rate in the summer. The percentage of the time for which dN/dh is less than -100 N-units/km is higher in the summer months of February and November, while lower in the winter months of May and August – and these values are higher than the corresponding β_0 estimates of ITU-R. dN/dh exceedances for a given percentage of an average year are closed to the ITU-R estimates. Also, the duct occurrence rate is seen to be much higher in summer than in winter. The occurrence rate for surface and elevated ducts is shown to be close to the ITU-R value for the region in the study. The median k is found to be is found to be 1.1, while the effective value of k exceeded 99.9% of the time is found to be 0.61.

CHAPTER FOUR

We note that the k-factor, derived in Chapter two, varies with refractivity, N, which in turn varies with temperature, pressure and humidity. It is necessary to know the variation of these primary parameters for Durban and Botswana. We therefore present plots of temperature, pressure and humidity variation with height, h, in the following sections. In addition, since k varies with refractivity gradient dN/dh, we also plot the values of dT/dh, dP/dh and de/dh as these define dN/dh.

4.1 Temperature Variation with Height

The temperature varies as the height increases above the ground level. The variation is either negative, (i.e. falling as height increases) or positive (increases as the height increases) depending on the season or months in question. While for some months temperature falls normally as the height rises above the ground level and in some other the reverse is the case. For this reason investigation has been carried out by working through all the months and seasons for both Durban and Botswana data. The variation of temperature with height for the two countries is shown in Figures 4.1 and 4.2.

The two Figures below show similarity in the distribution pattern for temperature variation with heights in the two countries, except for cases of temperature inversion[6] observed in some of the months. For the Durban data, temperature inversion is observed in the months of August and May, within the first 70m a.g.l (see Fig. 4.1). Temperature inversion is also observed for the month of August in Botswana (see Fig. 4.2).

The month of August therefore experiences temperature inversion in the two countries as observed from the figures below. It is therefore very important to make appropriate planning for temperature inversion, especially in the month of August as this is known to be the cause of ducting [see 11].

[6] Temperature inversion is when temperature increases with increase in height

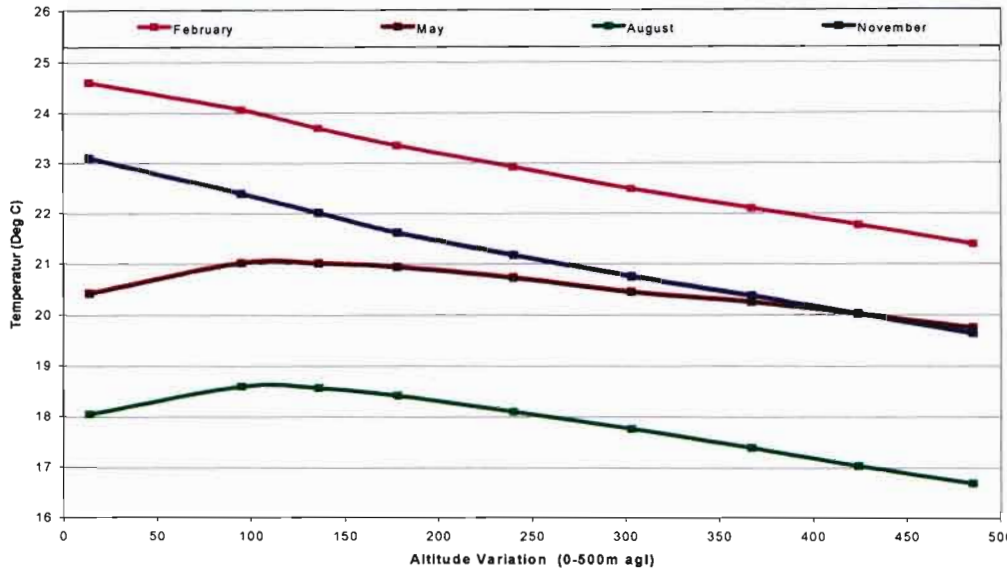

Fig. 4.1 Temperature Variation with Height for Durban [26]

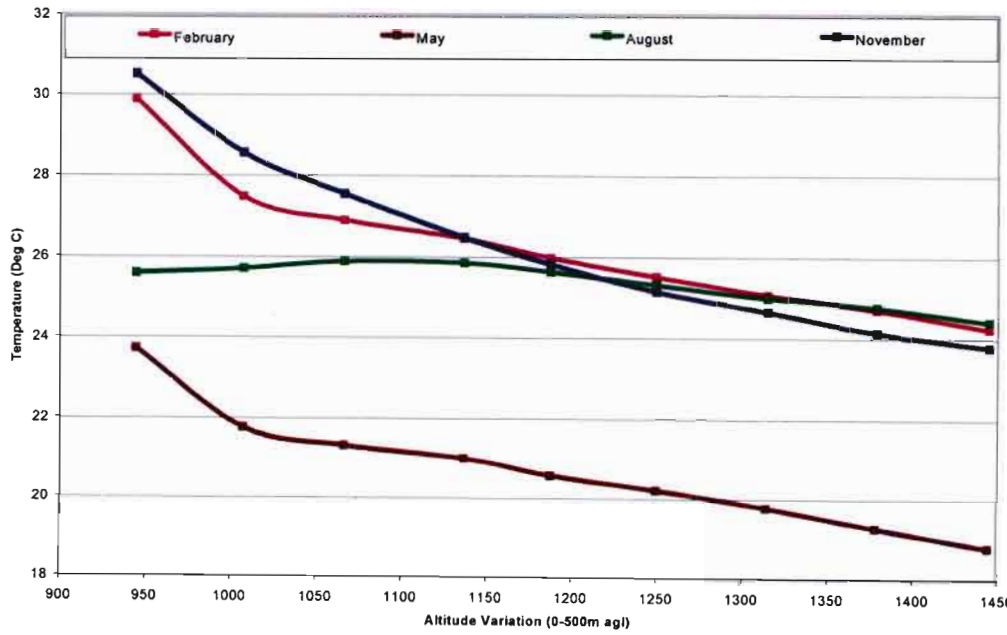

Fig. 4.2 Temperature Variation with Height for Botswana [27]

4.2 Pressure Variation with Height

With regards to variation of pressure as the altitude increases it is observed for all seasons, pressure value drops monotonically as height increases in both countries as expected. This is shown in figures 4.3 and 4.4. It is seen that the pressure gradient remains practically constant at about -0.1 mb/m for both Botswana and Durban.

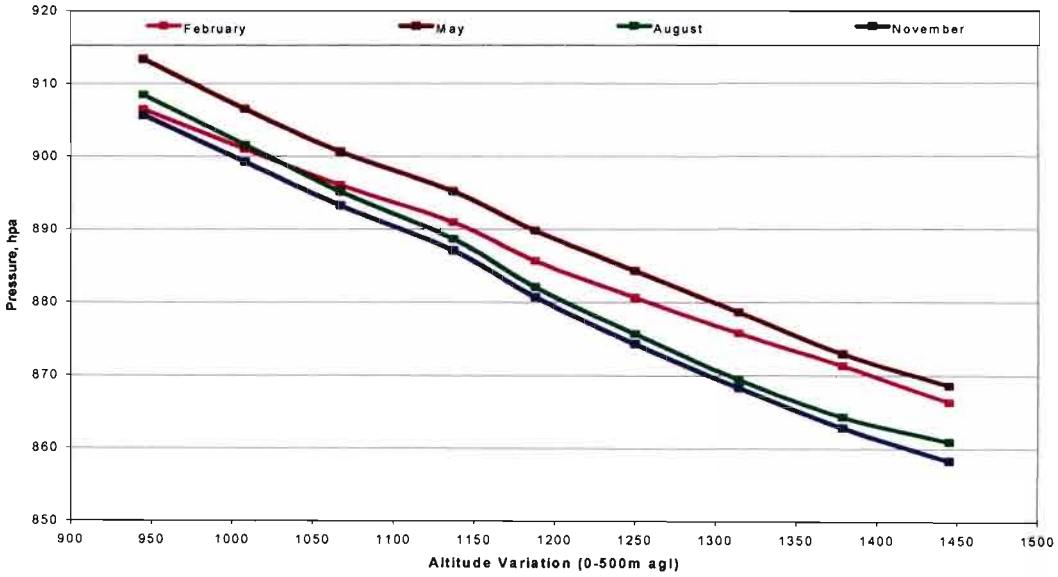

Fig. 4.3 Pressure Variation with Height for Botswana [27]

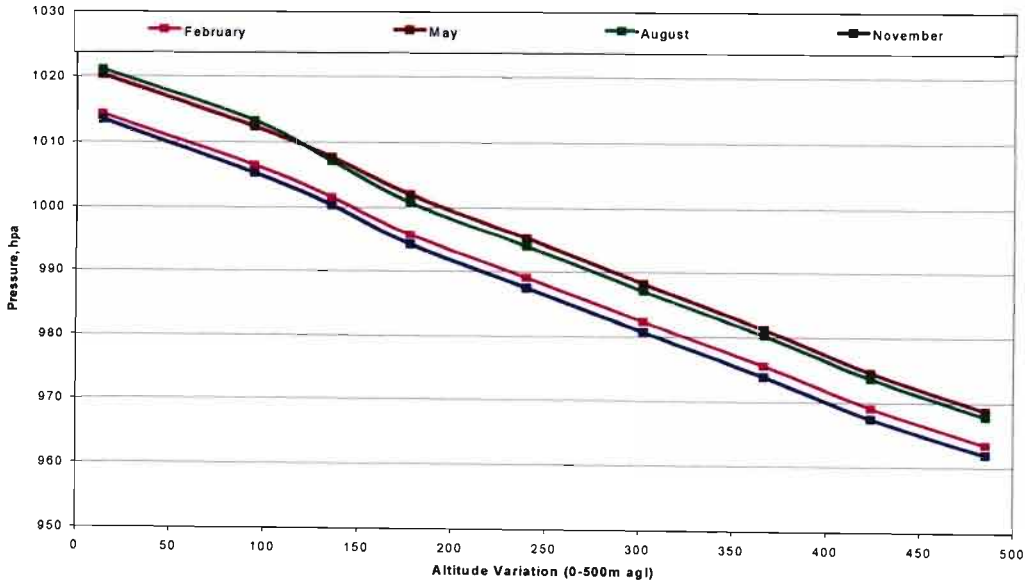

Fig. 4.4 Pressure Variation with Height for Durban [26]

4.3 Water Vapour Pressure Variation with Height

Water vapour also decreases as the altitude rises just like the case for other parameters. The two figures below give more insight into the behaviour of water vapour variation in Durban and Botswana. It can be observed that the humidity is higher for Durban when compared to Botswana. This is evident in the upper limit of water vapour as observed in the two figures. While the uppermost value for water vapour in Botswana (Maun is in the Kalahari Desert!) is observed to be below 10 hpa for all the seasons (see Fig.4.5), Durban is observed to record the highest value at about 25 hpa (see Fig. 4.6). Hence, one can convincingly say that Durban is more humid than Botswana as expected.

4.4 Temperature Gradient Variation with Height

Investigation carried out on temperature gradient variation with height shows that unlike the previous parameters these gradients have no regular pattern as the height increases for both countries. However, the average temperature gradient for Botswana was found to be -0.00090 °C/m for the winter month of August and November recorded an average gradient value of –0.0055 °C/m (see Fig.4.7). Meanwhile in Durban, the winter month of August recorded a higher temperature gradient of 0.0027 °C/m and November has a lower value of –0.0022 °C/m as shown in Fig.2.8.

4.5 Pressure Gradient Variation with Height

The average pressure gradient variation with height for Botswana is observed to be -0.06 hpa/m for the month of August while for the month of February it has a lower value of -0.081 hpa/m (see Fig. 4.9). In Durban, the average value of pressure gradient is 0.216 for the month of August while the month of February recorded a value of 0.115 (see Fig. 4.10).

4.6 Water Vapour Gradient Variation with Height

Average water vapour gradient in Botswana is -0.0025 hpa/m for the month of August while for the month of February the value drops to -0.0082 as shown in Fig. 4.11. In Durban, the average water vapour gradient for August is -0.00537 while for the month of May, the average value is observed to be -0.00537 (see Fig. 4.12). Note that the lowest gradient variation is within the first 10m a.g.l.

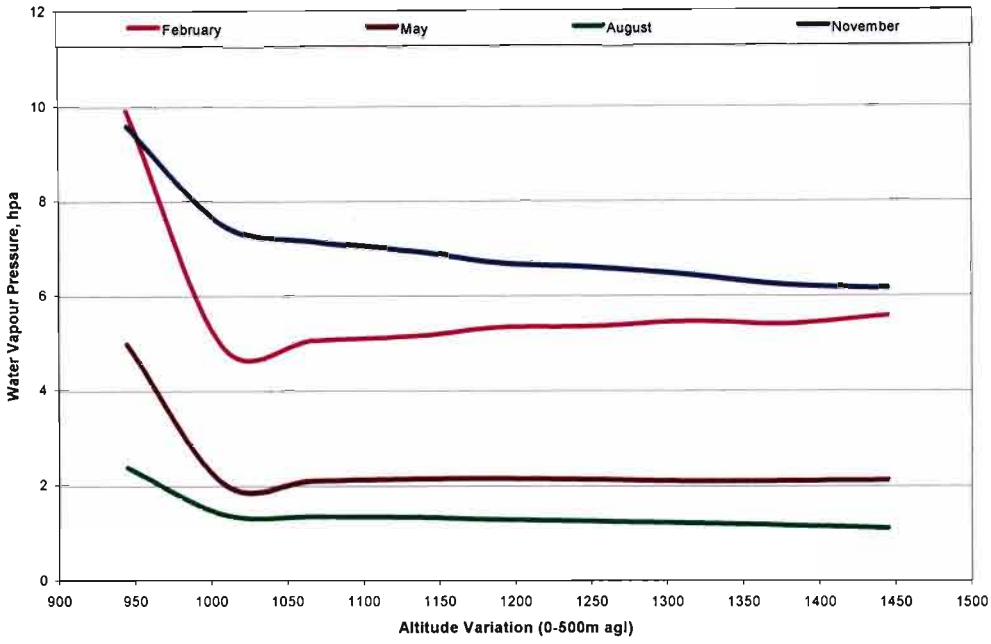

Fig. 4.5 Water Vapour Variation with Height for Botswana [27]

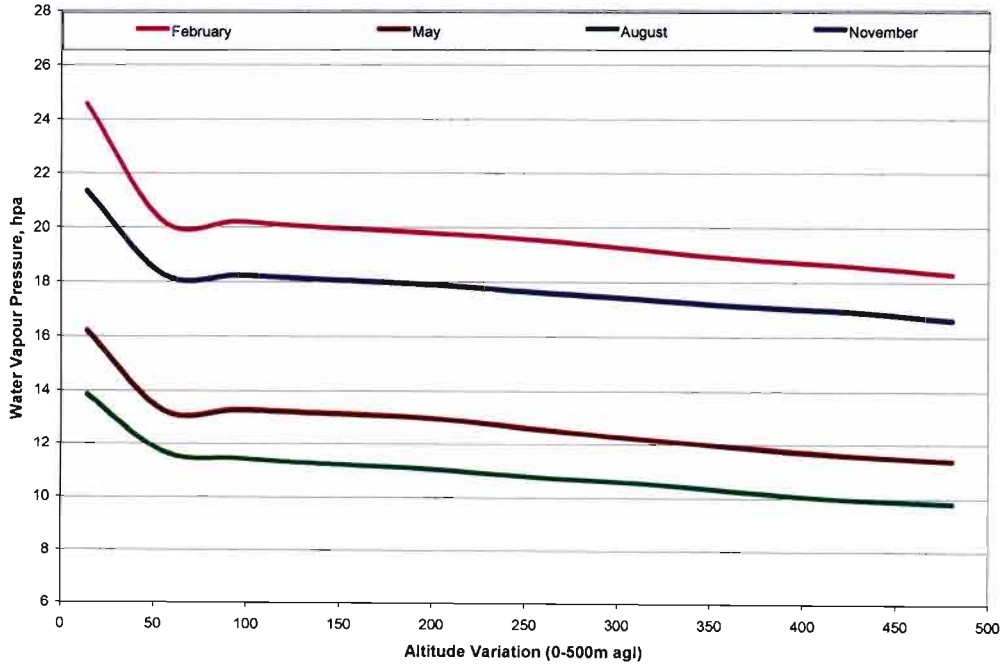

Fig. 4.6 Water Vapour Pressure Variation with Height for Durban [26]

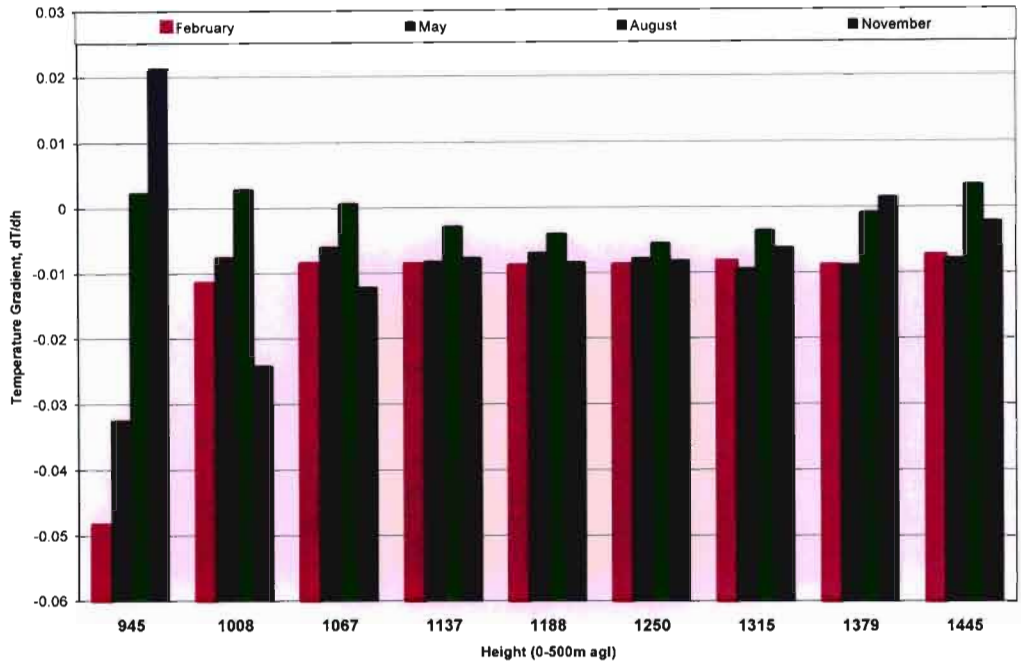

Fig. 4.7 Temperature Gradient Variation with Height for Botswana (average gradient for designated height range) [27]

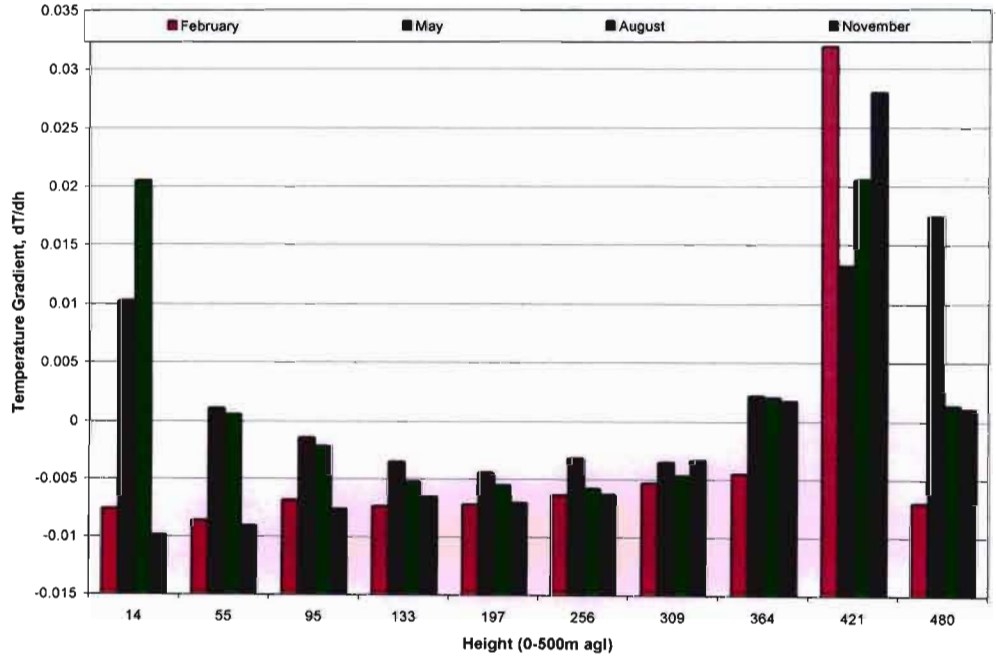

Fig. 4.8 Temperature Gradient Variation with Height for Durban (average gradient for designated height range) [26]

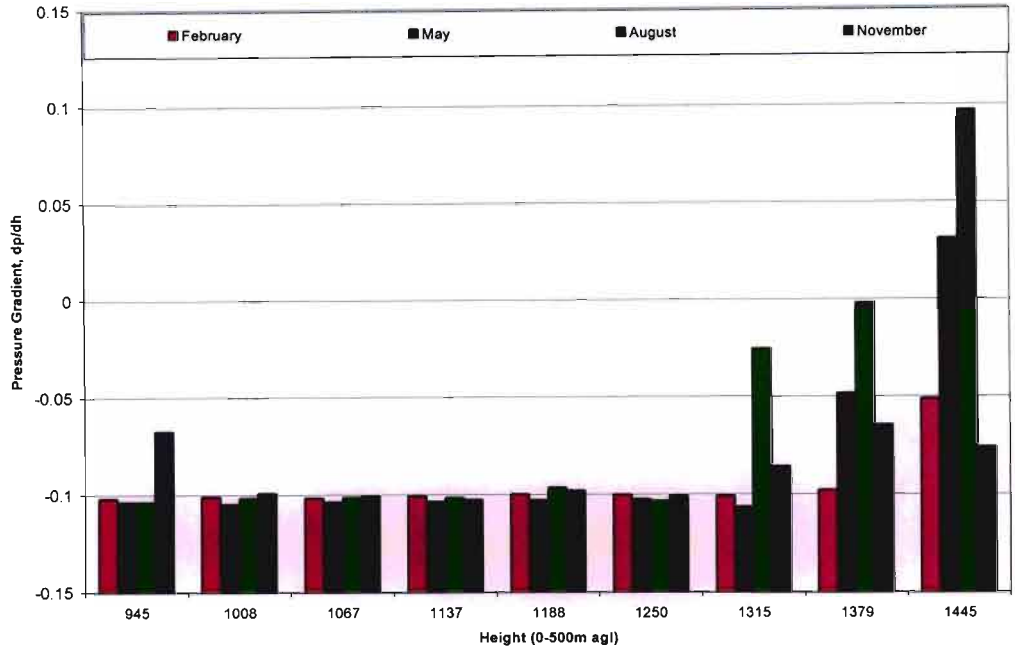

Fig. 4.9 Pressure Gradient Variation with Height for Botswana [27]

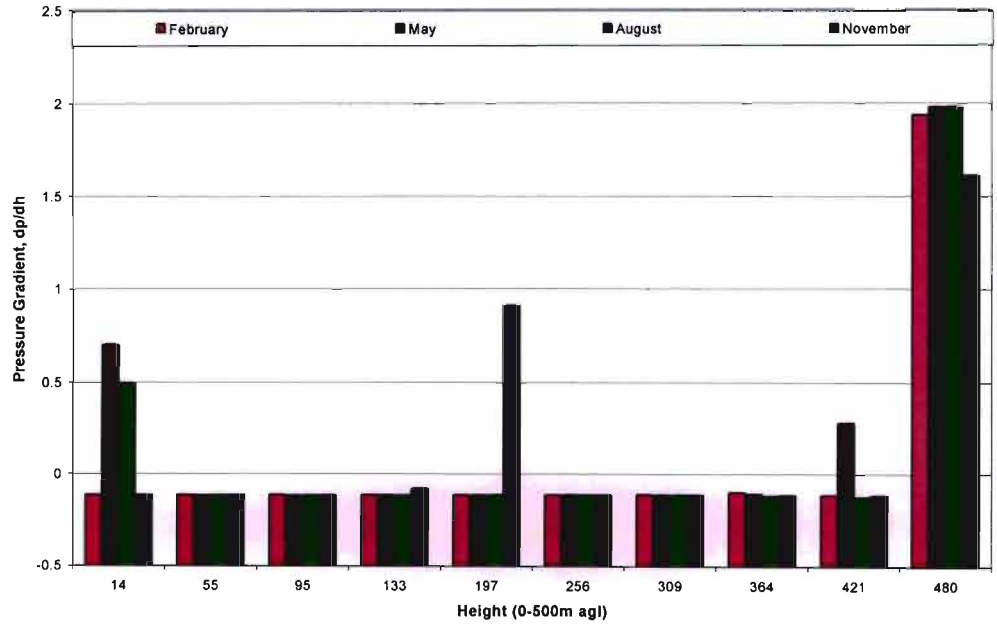

Fig. 4.10 Pressure Gradient Variation with Height for Durban [26]

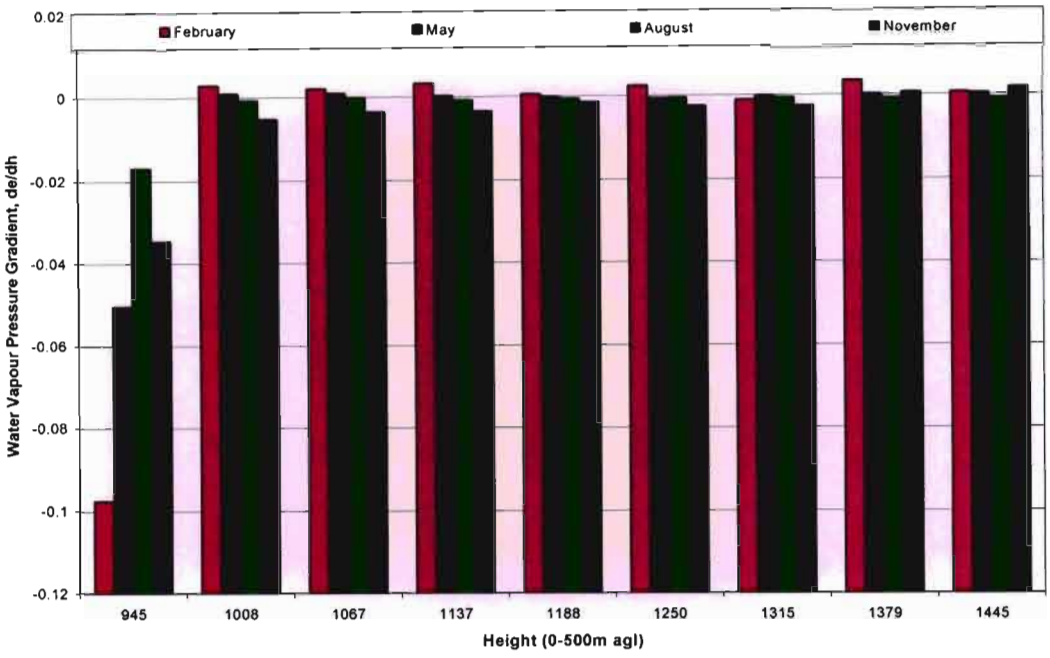

Fig. 4.11 Water Vapour Gradient Variation with Height for Botswana [27]

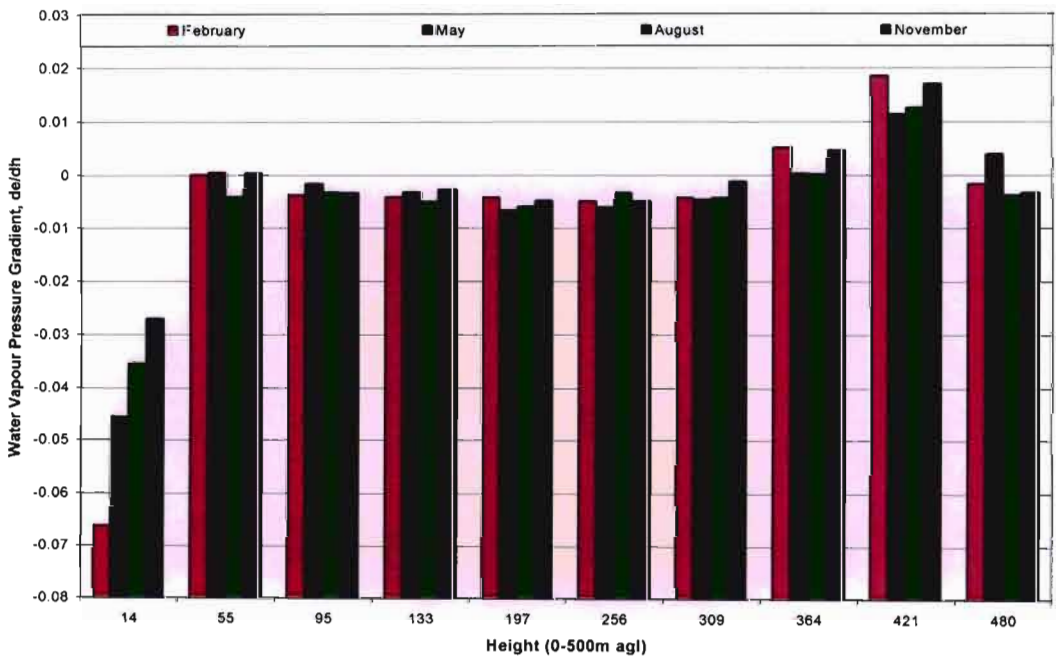

Fig. 4.12 Water Vapour Gradient Variation with Height for Durban [26]

4.7 Radio Refractivity Measurement

The discussions in this chapter have focused on the primary parameters of temperature, pressure and water vapour pressure. We note that k is determined from these via the refractivity gradient dN/dh. In this part, we briefly describe several ways of measuring refractivity, *N*.

4.7.1 Direct Method

In this method the microwave refractometer is used. It is capable of measuring rapid fluctuations in refractivity, *N*. The refractometer measures the change in the resonant frequency of a cylindrical cavity with ends open to the atmosphere and compares this with the resonant frequency of a standard cavity sealed from the atmosphere [23]. The refractometer is usually mounted on an aircraft for obtaining N-height profile; hence, it is an expensive technique.

4.7.2 Indirect Method

N can be computed from the measured pressure, temperature and water vapour pressure.

(i) Tethered balloon system can be used for height profile in the first km of the troposphere. It has poor time resolution because each profile can take up to 1hr [23].

(ii) Meteorological sensors can be installed at intervals on a tower for measurement of the three parameters pressure P, Temperature T, and water vapour pressure e. it is only applicable to the lowest 200m part of the atmosphere.

(iii) Upper air meteorological data measurements using radiosondes are carried out at some hundreds of stations all over the world with launches at 0000 hrs GMT and 1200 hrs GMT. This system provides a large volume of data for statistical analysis.

4.7.3 Sodar

This is an acoustic sound system, which is very useful for studying temperature inversions that cause radio ducts.

For the purpose of this research, the method used to gather the data was indirect method.

CHAPTER FIVE

5.1 Data Collation

The raw data, consisting of temperature, pressure, humidity, vapour pressure, saturated vapour pressure, dew point, wind speed, date, time etc, at varying altitude were collected and processed. Required parameters were sorted out and used, and the appropriate formulation was applied to calculate the refractivity gradient and eventually come up with the corresponding k-factors. The distribution curves for the k values were then plotted. Table 5.1 below shows a portion of the raw data for Botswana.

Table 5.1 Samples of Raw Data from Measurements in Botswana [27]

Altitude , m	Press, hPa	Temp, Deg C	RH, %	Dewp, deg C	Temp (K)	Sat,Vap Pres	Vap, Pres
945	904.5	27.00	57.0	17.8	300.0	20.40	11.63
1019	897.0	28.40	32.0	10.2	301.4	12.45	3.98
1077	891.1	28.10	32.0	9.9	301.1	12.20	3.90
1140	884.8	27.80	31.0	9.2	300.8	11.64	3.61
1194	879.5	27.30	31.0	8.7	300.3	11.25	3.49
1252	873.7	26.80	32.0	8.8	299.8	11.33	3.63
1299	869.0	26.50	31.0	8.1	299.5	10.81	3.35
1357	863.3	25.90	33.0	8.5	298.9	11.10	3.66
1407	858.4	25.50	33.0	8.1	298.5	10.81	3.57
1467	852.6	25.10	34.0	8.2	298.1	10.88	3.70
1518	847.6	24.60	34.0	7.8	297.6	10.59	3.60
1576	842.1	24.10	35.0	7.7	297.1	10.51	3.68
1640	835.9	23.50	36.0	7.6	296.5	10.44	3.76
1704	829.8	23.00	37.0	7.6	296.0	10.44	3.86
1767	823.8	22.50	38.0	7.5	295.5	10.37	3.94
1831	817.7	21.80	39.0	7.3	294.8	10.23	3.99
1895	811.8	21.20	41.0	7.5	294.2	10.37	4.25
1950	806.6	21.70	42.0	7.4	294.7	10.30	4.33
2013	800.7	20.20	43.0	7.3	293.2	10.23	4.40

The table represents one measurement in a day out of the thirty days in the month. Two measurements were performed daily and this was done for a twelve-month calendar period for three years. Hence the full data comprises of several such tables. There is therefore the need to

sort the data so that important parameters can be extracted. The aim is to calculate k-factor values and its distribution based on these measurements. The various processes embarked upon to sort the data were highlighted in the succeeding sections.

For Durban, like Botswana radiosonde data was downloaded from the South African Weather Services database. Hence, the raw data comprises of many parameters including those not needed. A Visual Basic software developed in [11] was used to sort the data into an excel format. A snapshot of the raw data from the weather department is displayed in Fig.5.1.

SynopNo,DateT,Time of release,DeltaT,Pressure,Temp,Hum,Dewpt,GPM,Winddir,Windsp,68588,2003/11/26,10:42:00AM,0,1009.6,25.6,72,20.2,14.0,190,6.0
SynopNo,DateT,Time of release,DeltaT,Pressure,Temp,Hum,Dewpt,GPM,Winddir,Windsp,68588,2003/11/26,10:42:00AM,10,1000.2,23.1,68,16.9,95.0,,
SynopNo,DateT,Time of release,DeltaT,Pressure,Temp,Hum,Dewpt,GPM,Winddir,Windsp,68588,2003/11/26,10:42:00AM,20,995.6,22.4,69,16.5,136.0,,
SynopNo,DateT,Time of release,DeltaT,Pressure,Temp,Hum,Dewpt,GPM,Winddir,Windsp,68588,2003/11/26,10:42:00AM,30,990.7,21.8,72,16.5,178.0,,
SynopNo,DateT,Time of release,DeltaT,Pressure,Temp,Hum,Dewpt,GPM,Winddir,Windsp,68588,2003/11/26,10:42:00AM,40,983.7,21.3,75,16.7,240.0,,
SynopNo,DateT,Time of release,DeltaT,Pressure,Temp,Hum,Dewpt,GPM,Winddir,Windsp,68588,2003/11/26,10:42:00AM,50,976.6,20.6,77,16.4,303.0,,
SynopNo,DateT,Time of release,DeltaT,Pressure,Temp,Hum,Dewpt,GPM,Winddir,Windsp,68588,2003/11/26,10:42:00AM,60,969.4,20.1,81,16.7,367.0,,
SynopNo,DateT,Time of release,DeltaT,Pressure,Temp,Hum,Dewpt,GPM,Winddir,Windsp,68588,2003/11/26,10:42:00AM,70,963.1,19.6,82,16.5,424.0,,
SynopNo,DateT,Time of release,DeltaT,Pressure,Temp,Hum,Dewpt,GPM,Winddir,Windsp,68588,2003/11/26,10:42:00AM,80,956.3,19.4,77,15.3,485.0,,

Fig. 5.1 Snapshot of the raw data for Durban [26]

5.2 Data Sorting

On close examination of table 5.1 above, it can be observed that the altitude is between 945m to 2013m above the sea level, the full data actually goes up to 6,000m above sea level. This is far beyond our requirements of 0-200m and 0-500m a.g.l ranges. So the first thing that was done was

to sort the data one after the other so that the height ranges 0-200m and 0-500m can be extracted from the original raw data.

Meanwhile for the Durban data, the visual basic code developed in [11] was used to re-read the data from the snapshot in Fig. 5.1 to a standard excel sheet format for easy processing. A portion of the visual basic code included in the appendix. After the data had been taken through the visual basic code, the result was a secondary data shown in Table 5.2.

Table 5.2 Secondary Raw Data for Durban [from Fig. 5.1]

Date & Time	Height	Pressure	Temperature	Humidity	Refractivity	Refractive Index
2003/11/26 - 10:42:00AM	14	1009.6	25.60	72.0	361.1	1.000361
2003/11/26 - 10:42:00AM	95	1000.2	23.10	68.0	343.6	1.000343
2004/08/31 - 11:10:00PM	260	987.6	18.20	90.0	345.7	1.000345
2004/08/31 - 11:10:00PM	321	980.6	17.70	95.0	346.4	1.000346
2004/08/31 - 11:10:00PM	379	973.9	17.20	99.0	346.2	1.000346
2004/08/31 - 11:10:00PM	438	967.3	16.90	97.0	341.6	1.000341

After collating the data in the excel format as shown in table 5.2 above, the data was then broken into the constituent months so that there are ten separate files instead of having the whole data for the ten months period in one file. This was done so that the analysis can be easier and the work can be done on a monthly and seasonal basis. There are therefore ten excel sheet that look like the format of Table 5.2.

5.3 The k-factor Calculation

k values were calculated for the different height ranges for both Durban and Botswana. The procedure used for the calculation is as follows: For Botswana, the data in table 5.1 were sorted for different months of the year for a three-year period and then merged into two folders to reflect the different height ranges of 0-200m a.g.l. and 0-500m a.g.l. k values for these height ranges were then calculated using the appropriate formulation as shown in Tables 5.3 and 5.4.

Table 5.3 Calculated k-factors for Height 0-200m a.g.l., Botswana [From Table 5.1]

Altitude, m	K-factor
945	-0.49
1019	1.21
1077	1.35
1140	1.20
1194	1.06

Table 5.4 Calculated k-factors, for Height 0-500m a.g.l., Botswana [From Table 5.1]

Altitude, m	K-factor
945	-0.49
1019	1.21
1077	1.35
1140	1.20
1194	1.05
1252	1.40
1299	0.96
1357	1.20
1407	1.06
1467	1.19

Meanwhile for Durban, the refractivity column of table 5.2 was extracted for each of the ten months to do the calculation. These were collated in different excel sheet and the result of the exercise is shown in Table 5.5. It must be noted that the result displayed in table 5.5. is only for the month of April 2004. Similar tables were developed for the other nine months. These are not included here for space consideration. These were sorted into different height ranges and then processed separately.

Table 5.5. K-Factor Calculation for Durban [See Fig. 5.1 and Table 5.2]

Date & Time	Height	dh	Refractivity, N	dN	dN/dh	k-factor
2004/04/01 - 10:49:00AM	14	41	352.9	-21.6266	-0.5275	-0.42
2004/04/01 - 10:49:00AM	55	40	331.3	1.3260	0.0332	0.82
2004/04/01 - 10:49:00AM	95	38	332.6	-2.2411	-0.0589	1.60
2004/04/01 - 10:49:00AM	421	59	322.6	-2.0794	-0.0352	1.05
2004/04/01 - 10:49:00AM	480	-480	320.6	-320.5717	0.6678	1.28

5.4 The k-factor Processing

After the k-factor had been calculated for both Botswana and Durban, the probability distribution for the k-factor was then processed. This was done by extracting the k-factor calculated in the previous section and uses it to calculate the probability distribution. The intermediate process is the calculation of occurrence frequency and cumulative distribution function (CDF) as shown in Tables 5.6 and 5.7.

Table 5.6 k-Factor Distribution, Botswana (portion of data for one Season)

k-factor Distrbtn for 500m	k-ranges	Occurrence Frequency	Probability of Occurrence	Probability (k<ki)=F(ki)	pdf, f(ki)
-0.27	-8.00	15	0.0095	0.0095	0.00
0.93	-7.99	0	0.0000	0.0095	0.00
1.24	1.10	51	0.0324	0.3989	3.11
0.91	1.11	49	0.0311	0.4301	2.66
3.36	1.12	42	0.0266	0.4567	1.84
2.35	7.97	0	0.0000	1.0000	0.00
-1.53	7.98	0	0.0000	1.0000	0.00
1.58	7.99	0	0.0000	1.0000	0.00
3.30	8.00	0	0.0000	1.0000	0.00

Table 5.7 k-factor Distribution, South Africa (portion of data for one Season)

k-factor Distrbtn 500m	k-ranges	Occurrence Frequency	Probability of Occurrence	Probability (k<ki)=F(ki)	pdf, f(ki)
1.00	-5.00	8	0.0181	0.0181	0.00
0.99	-4.99	0	0.0000	0.0181	0.00
0.98	-4.98	0	0.0000	0.0181	0.00
0.51	1.19	8	0.0181	0.2454	1.36
0.21	1.20	6	0.0136	0.2590	1.13
-1.20	1.21	5	0.0113	0.2704	1.81
0.12	4.98	0	0.0000	1.0000	0.00
-1.51	4.99	0	0.0000	1.0000	0.00
2.31	5.00	0	0.0000	1.0000	0.00

Tables 5.6 and 5.7 above show few sample data for analysis at this stage. It should be noted that the beginning and the end of the sample data is shown in the table, this is the reason for having the initial row for k-range to be -8 and the final row +8 (see table 5.6).

5. 5 Results for Botswana and Durban

From the analysis carried out in the previous sections, different results that predict the distribution of the k-factor for both data were obtained. Initially, the k-factor distribution for different months and different seasons were merged into a table for the whole year for both Botswana and Durban. The occurrences of the ranged values of k from the raw values of k were plotted for both Botswana and Durban (see Fig. 5.2 – 5.3).

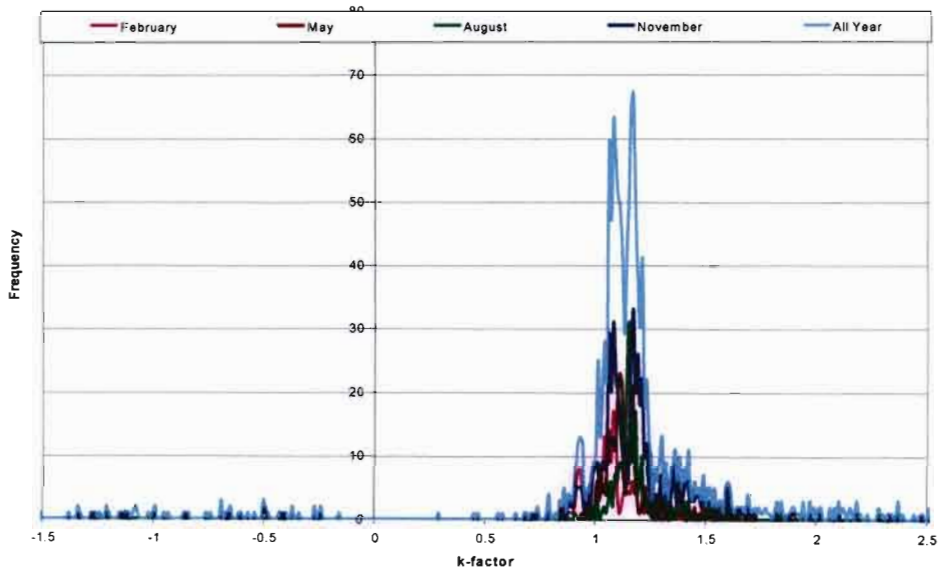

Fig. 5.2 Occurrence Frequency Distribution for all seasons and all year (0-500m), Botswana

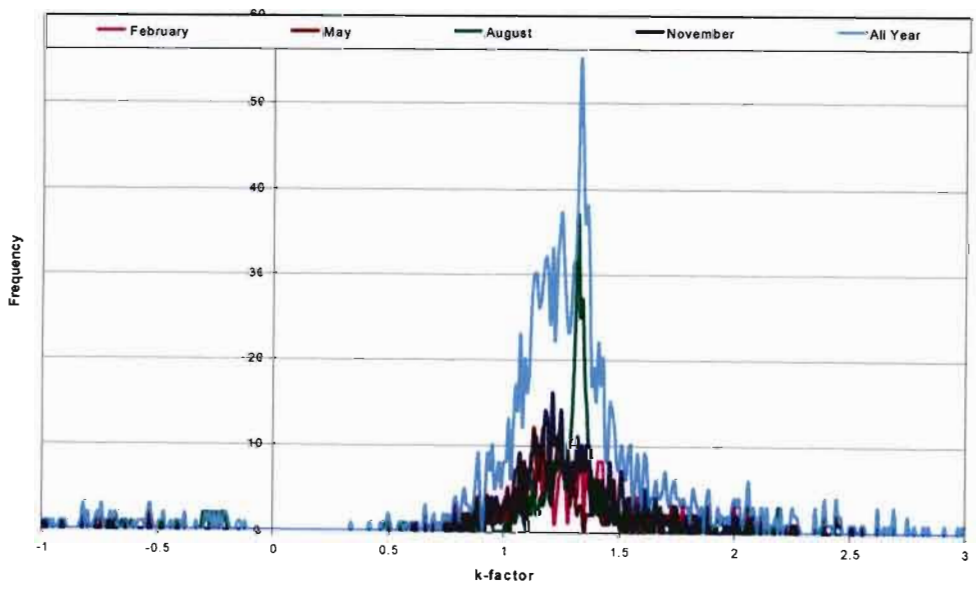

Fig.5.3 Occurrence Frequency Distribution for all seasons and all years (0-500m), Durban

The cumulative distribution function curves were plotted in both countries for the two data sets. These are displayed in figures 5.4-5.5.

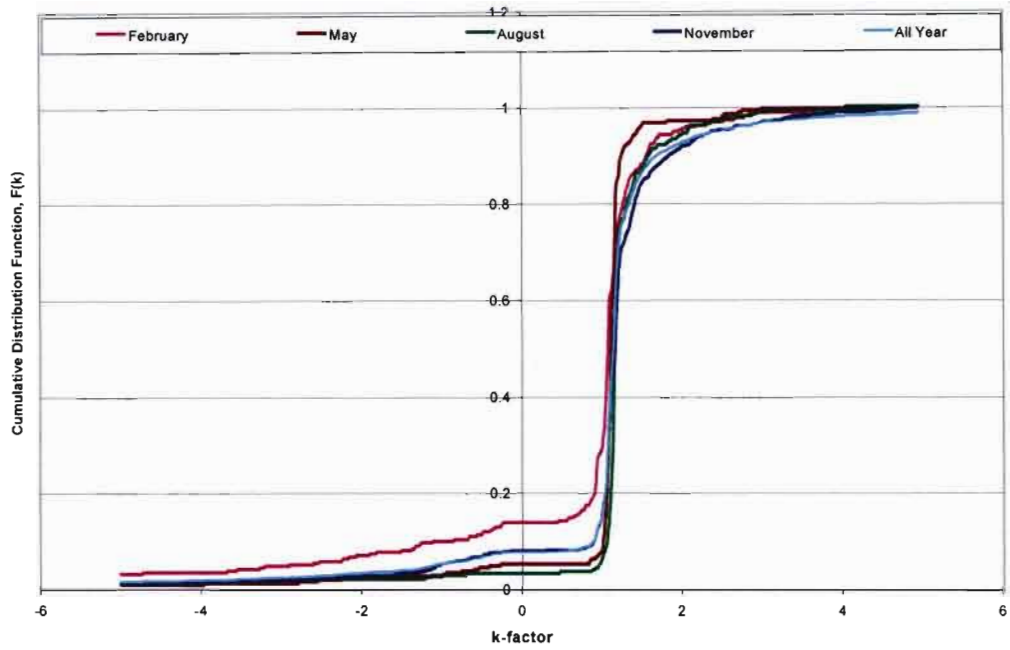

Fig. 5.4 Cumulative Distribution plot for all seasons and all years, (0-500m agl), Botswana.

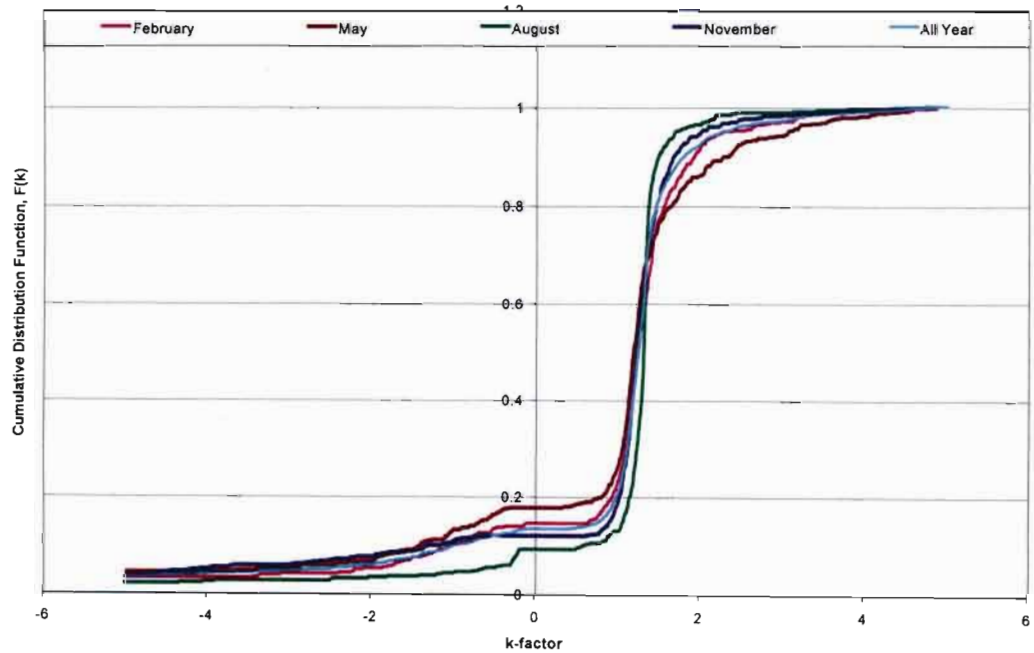

Fig. 5.5 Cumulative Distribution plot for all seasons and all years, (0-500m agl), Durban.

Finally the probability density function curves were plotted for the two data sets, these are shown in figures 5.6-5.7.

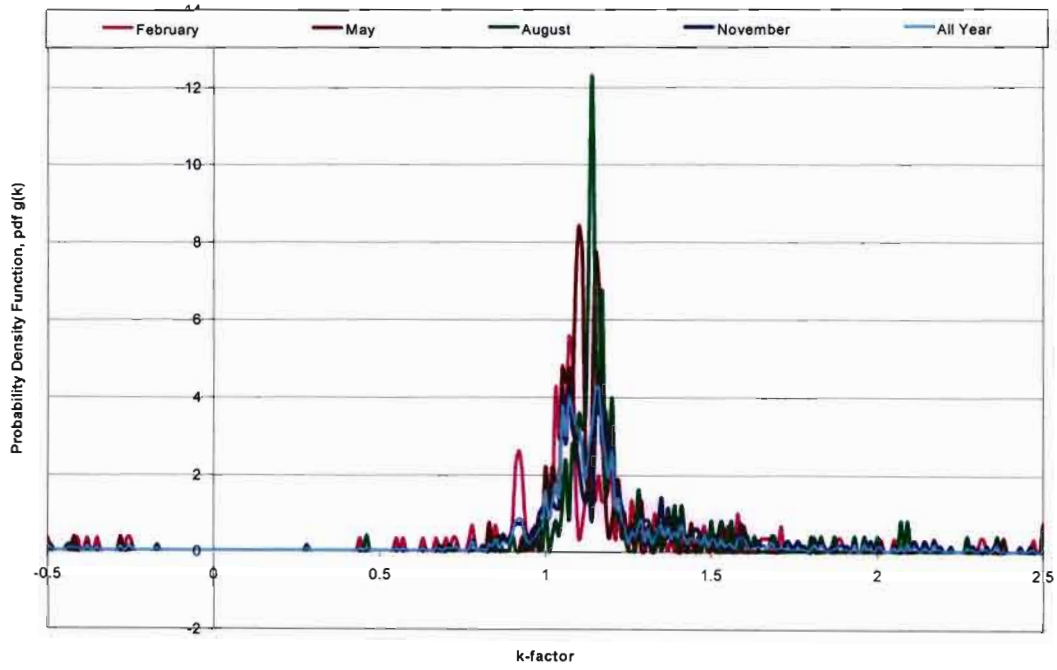

Fig. 5.6. Probability Density Function plot for all seasons and all years, (0-500m agl), Botswana.

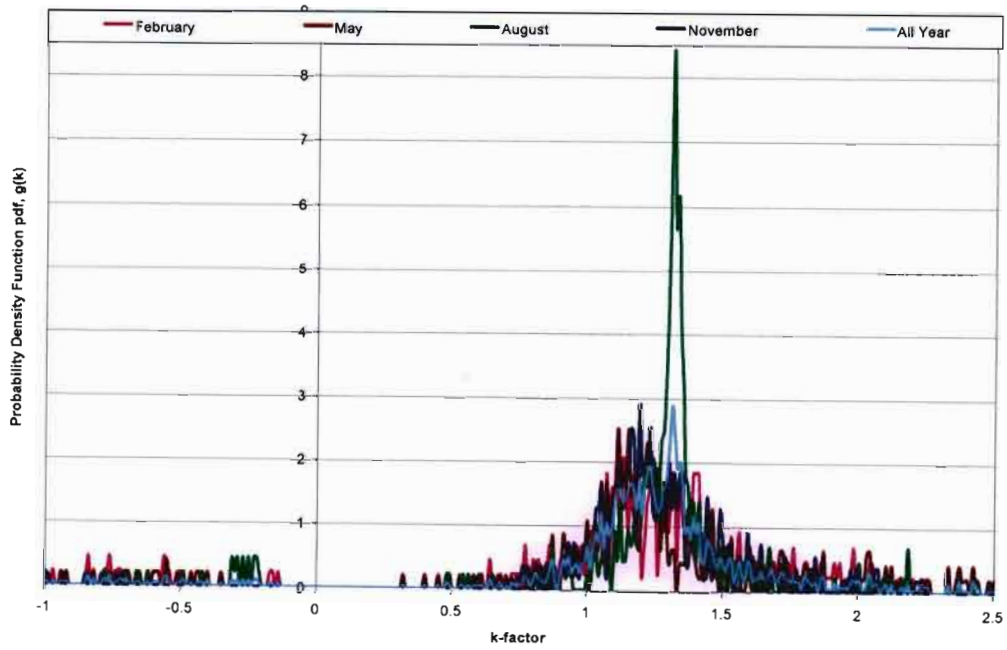

Fig. 5.7 Probability Density Function plot for all seasons and all years, (0-500m agl), Durban.

5.6 Estimates of the k-factor pdf

The curve fitting process for probability density function, pdf, was done next for each of the data set so as to make true estimates of the curves and get the appropriate k-factor values for each of the data. The curve fitting process was done using the proposed model and algorithm described earlier in section 2.6. The result of this is shown in figures 5.8-5.17.

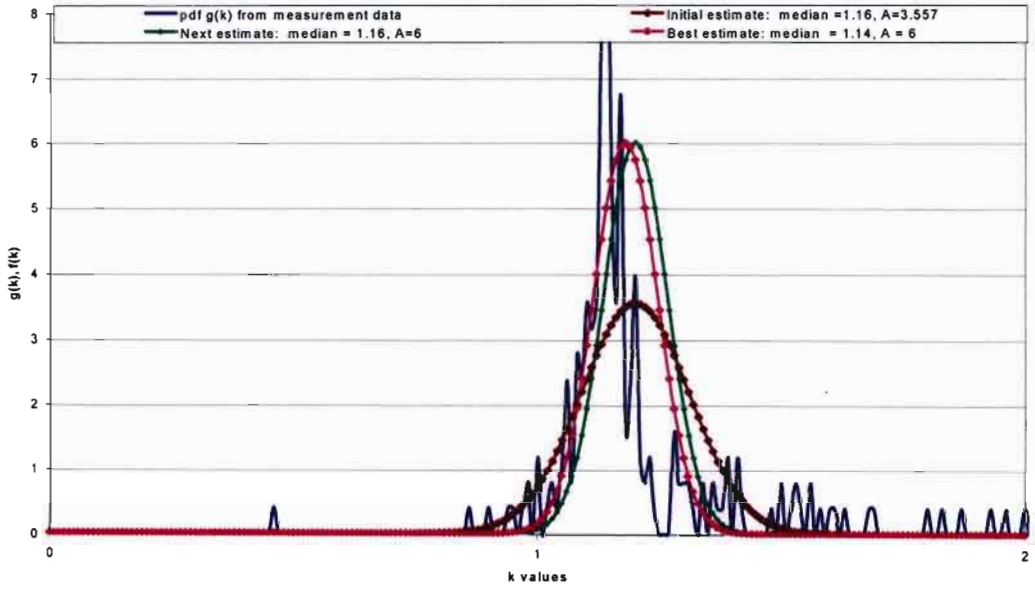

Fig. 5.8 Measured and estimated pdf g(k) and f(k), August (0-500m a.g.l.) Botswana

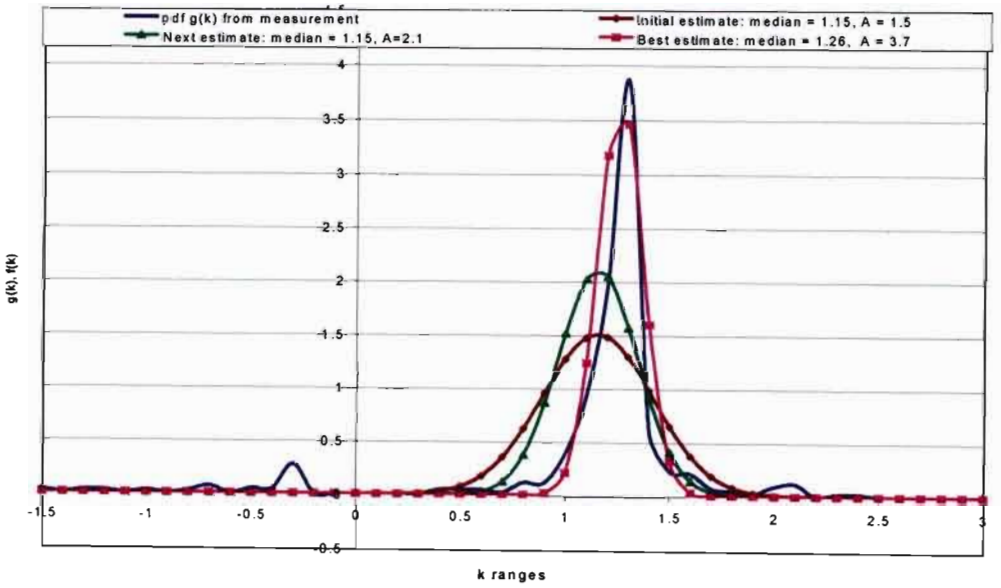

Fig. 5.9 Measured and estimated pdf g(k) and f(k), August (0-500m a.g.l.) Durban

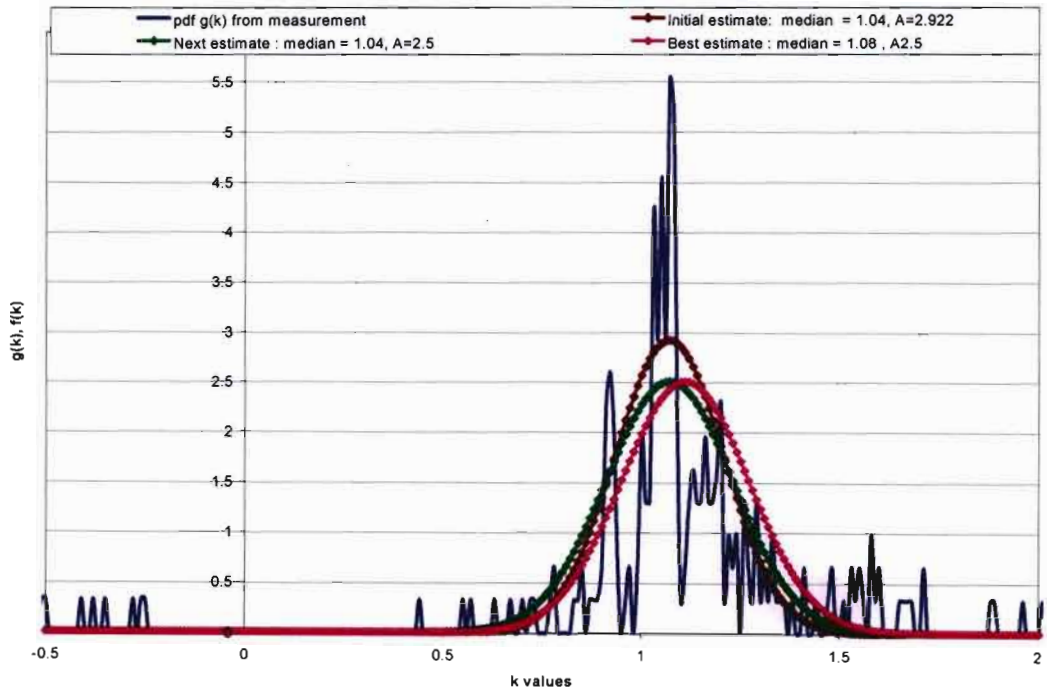

Fig. 5.10 Measured and estimated pdf g(k) and f(k) February (0-500m a.g.l.) Botswana

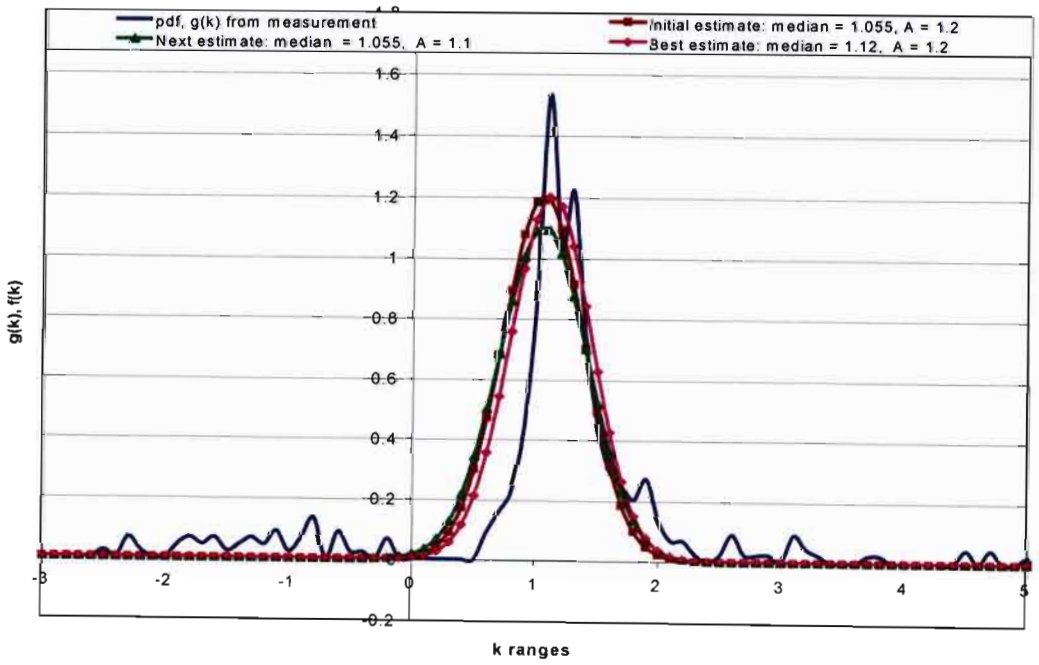

Fig. 5.11. Measured and estimated pdf, g(k) and f(k) February (0-500m a.g.l.) Durban.

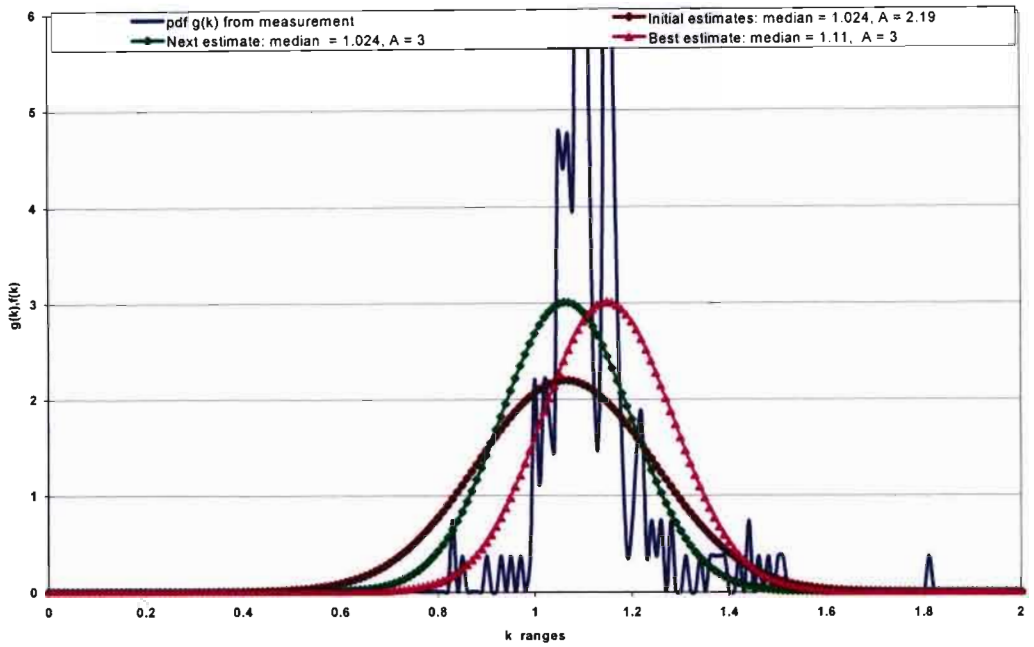

Fig. 5.12 Measured and estimated pdf g(k) and f(k) May (0-500m a.g.l.) Botswana.

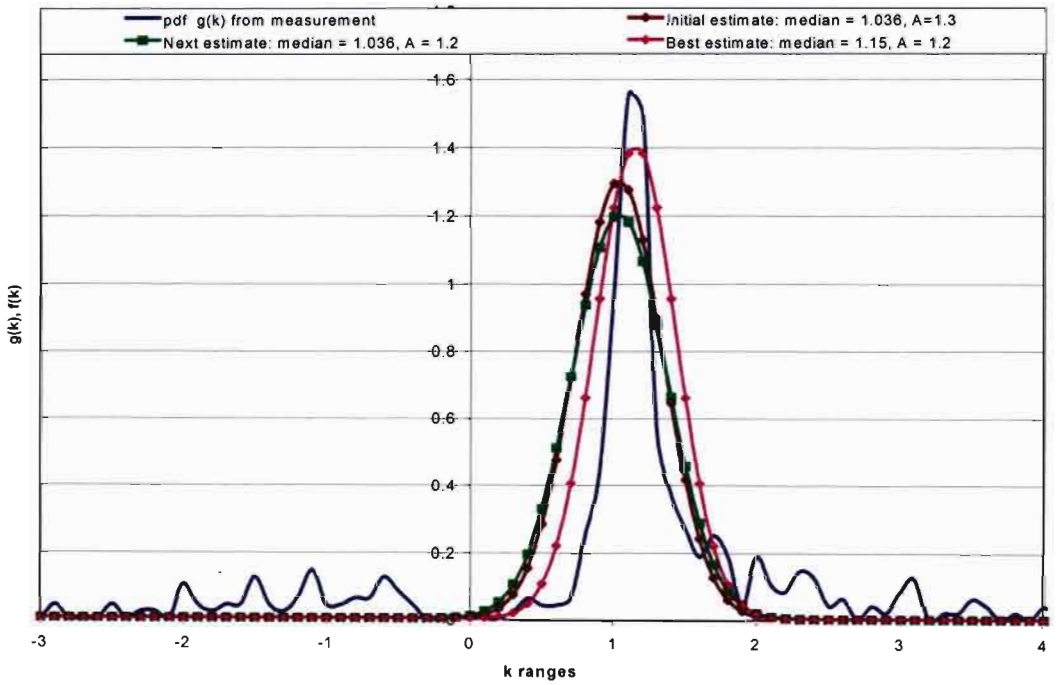

Fig. 5.13 Measured and estimated pdf g(k) and f(k) May (0-500m a.g.l.) Durban.

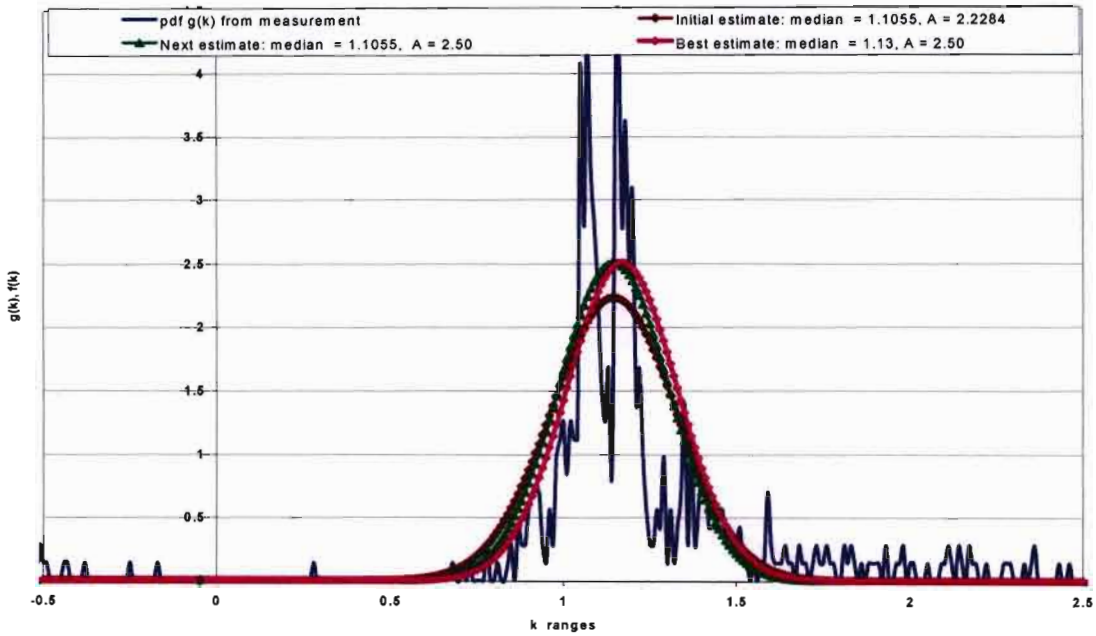

Fig. 5.14 Measured and estimated pdf g(k) and f(k) November (0-500m a.g.l.) Botswana

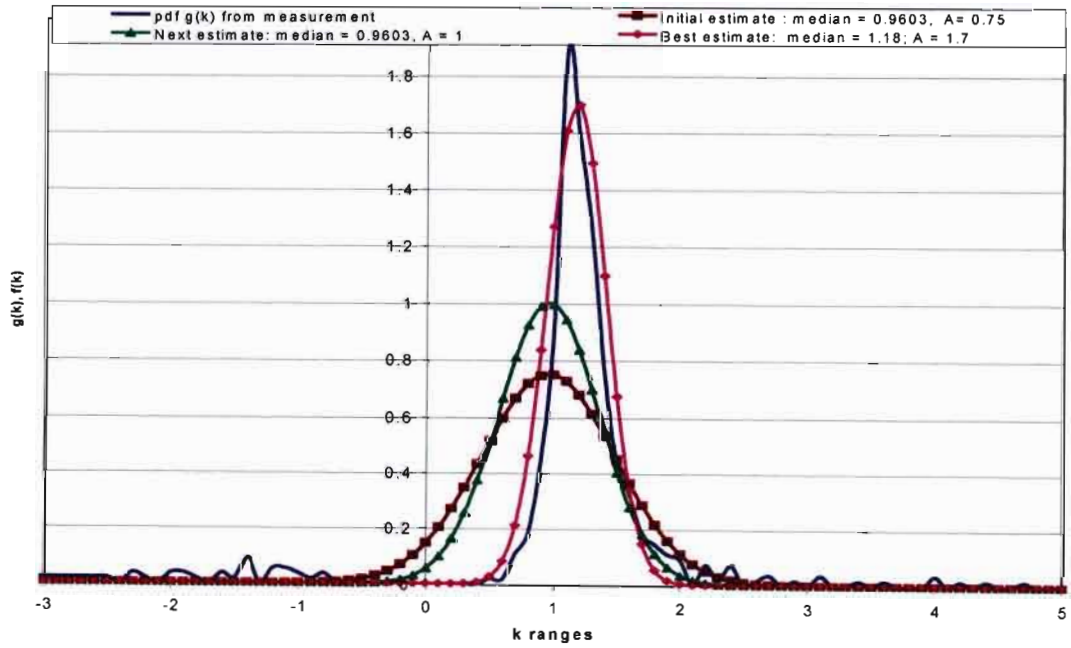

Fig. 5.15 Measured and estimated pdf g(k) and f(k) November (0-500m a.g.l.) Durban.

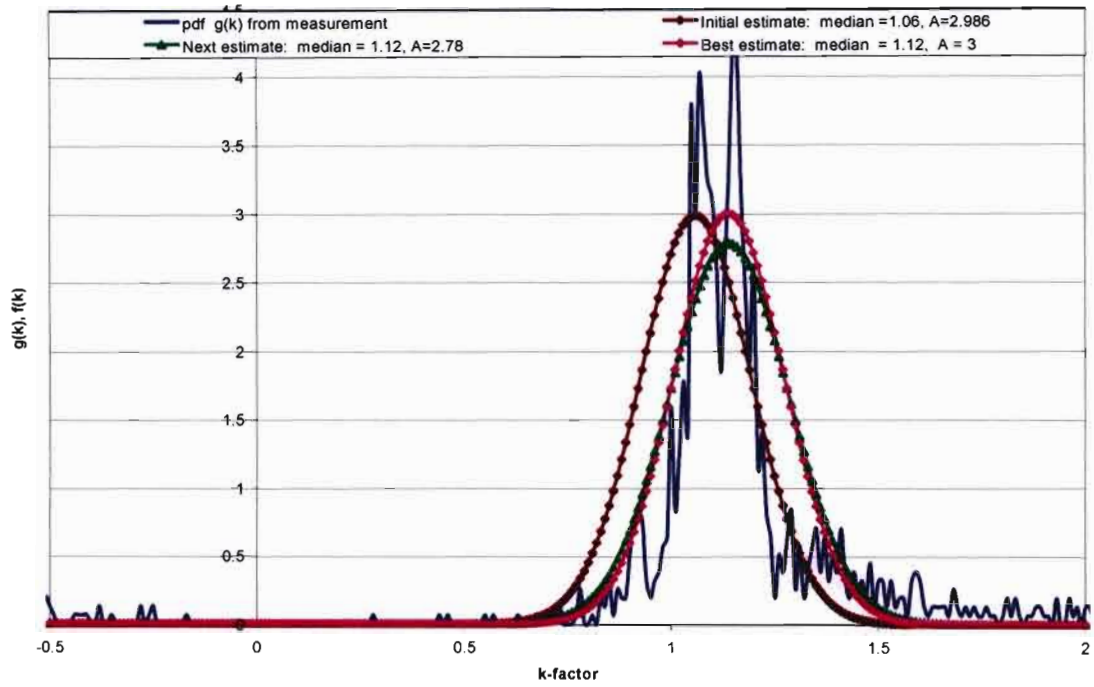

Fig. 5.16 Measured and estimated pdf g(k) and f(k) All Year (0-500m a.g.l.) Botswana.

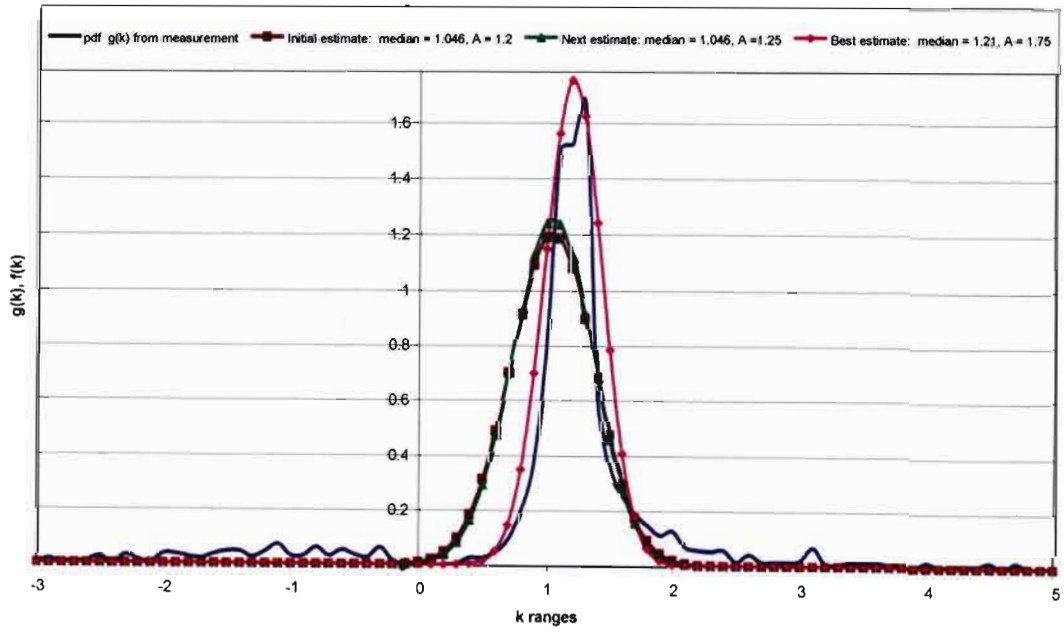

Fig. 5.17 Measured and estimated pdf g(k) and f(k) All Year (0-500m a.g.l.) Durban

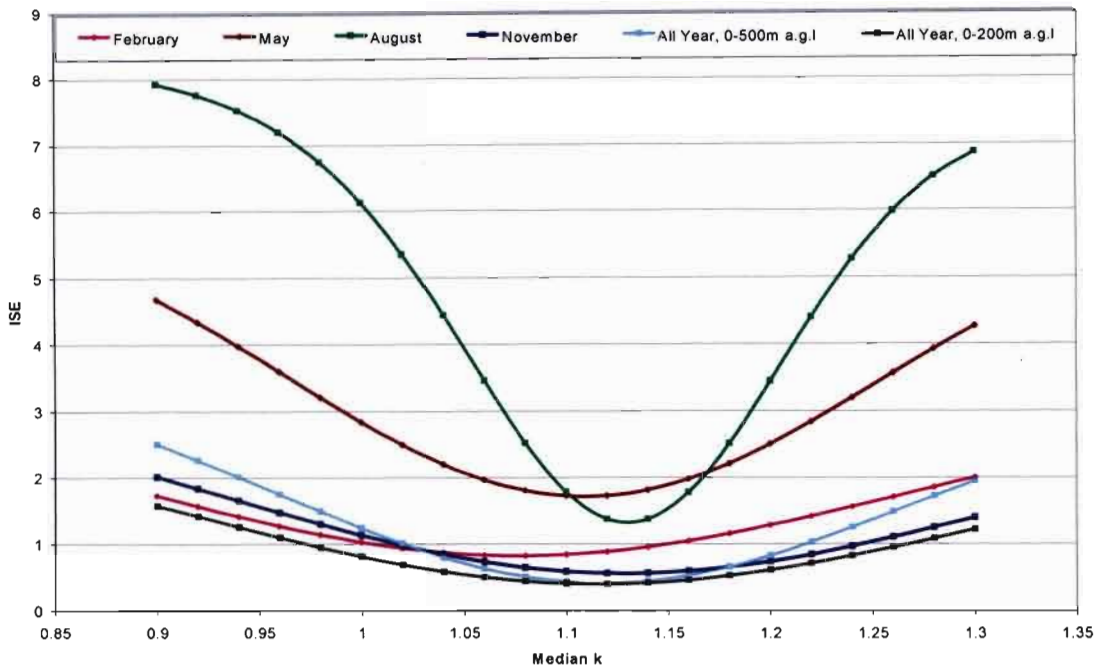

Fig.5.18 Variation of Median k, μ_k with Integral of Square Error (ISE) for Botswana

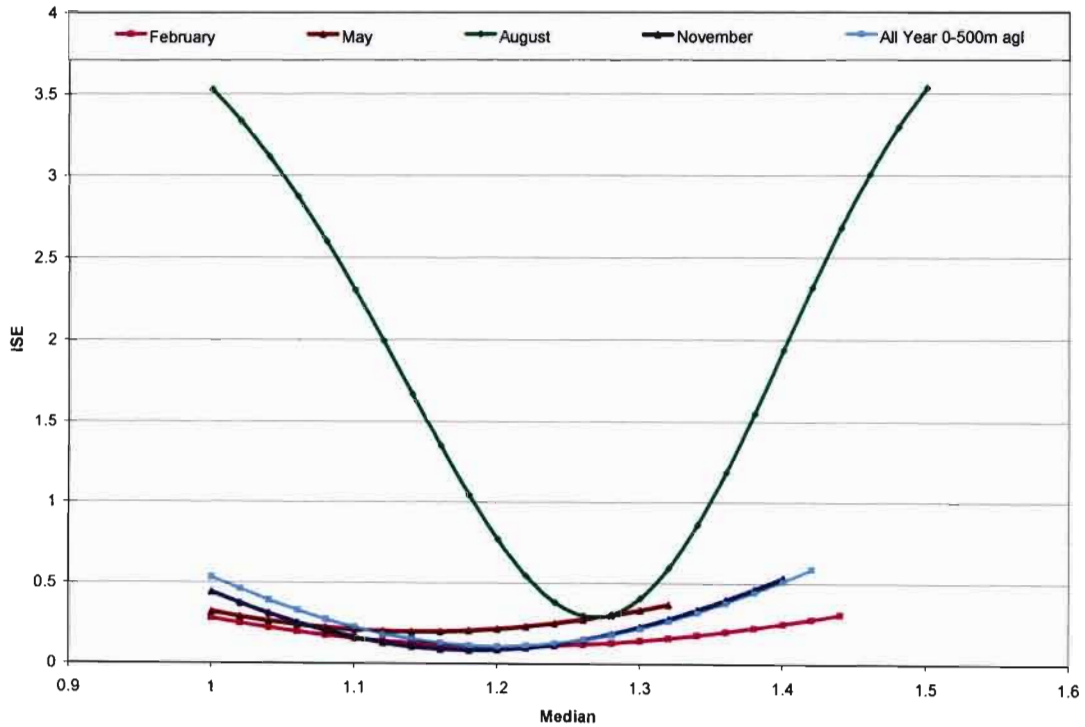

Fig. 5.19 Variation of Median k, μ_k with Integral of Square Error (ISE) for Durban

Table 5.8 Values of μ_k, A, and ISE for Botswana

Period	Initial measurements estimates, g(k)			Next measurement estimates from calculation, f(k)			Final estimates from calculation, optimum f(k)		
	μ_k	A	ISE	μ_k	A	ISE	μ_k	A	ISE
February (0-500m a.g.l.)	1.04	2.92	0.891	1.05	2.50	0.858	1.08	2.50	0.810
May (0-500m a.g.l.)	1.02	2.19	2.560	1.02	3.00	2.424	1.11	3.00	1.705
August (0-500m a.g.l.)	1.16	3.55	1.892	1.16	6.00	1.766	1.14	6.00	1.358
November (0-500m a.g.l.)	1.10	2.22	0.591	1.10	2.50	0.570	1.13	2.50	0.550
All Year (0-500m a.g.l.)	1.06	2.98	0.616	1.12	2.78	0.421	1.12	3.00	0.398
All Year (0-200m a.g.l.)	1.15	1.00	0.636	1.12	3.00	0.455	1.12	2.50	0.402

Table 5.9 Values μ_k, A, and ISE for Durban

Period	Initial measurements estimates, g(k)			Next measurement estimates from calculation, f(k)			Final estimates from calculation, optimum f(k)		
	μ_k	A	ISE	μ_k	A	ISE	μ_k	A	ISE
February (0-500m a.g.l.)	1.05	1.20	0.192	1.05	1.10	0.189	1.12	1.20	0.129
May (0-500m a.g.l.)	1.03	1.30	0.253	1.03	1.20	0.251	1.15	1.40	0.189
August (0-500m a.g.l.)	1.15	1.50	0.938	1.15	2.10	0.856	1.26	3.70	0.291
November (0-500m a.g.l.)	0.96	0.75	0.445	0.96	1.00	0.411	1.18	1.70	0.077
All Year (0-500m a.g.l.)	1.04	1.20	0.287	1.04	1.25	0.287	1.21	1.75	0.099

Figures 5.8- 5.17 give plots of measured and estimated values, g(k) and f(k) as k varies.

The optimum distributions for Botswana are determined to be:

$$\left.\begin{array}{ll}
\text{February (0 - 500m a.g.l.)} & f(k) = 2.5e^{-19.63(k-1.08)^2} \\
\text{May (0 - 500m a.g.l.)} & f(k) = 3e^{-28.28(k-1.11)^2} \\
\text{August (0 - 500m a.g.l.)} & f(k) = 6e^{-113.12(k-1.14)^2} \\
\text{November (0 - 500m a.g.l.)} & f(k) = 2.5e^{-19.63(k-1.13)^2} \\
\text{All Year (0 - 500m a.g.l.)} & f(k) = 3e^{-28.28(k-1.12)^2} \\
\text{All Year (0 - 200m a.g.l.)} & f(k) = 2.5e^{-19.63(k-1.12)^2}
\end{array}\right\} \quad (5.1)$$

The optimum distributions for Durban are as follows:

$$\left.\begin{array}{ll}
\text{February (0 - 500m a.g.l.)} & f(k) = 1.2e^{-4.52(k-1.12)^2} \\
\text{May (0 - 500m a.g.l.)} & f(k) = 1.4e^{-6.16(k-1.15)^2} \\
\text{August (0 - 500m a.g.l.)} & f(k) = 3.7e^{-43.01(k-1.26)^2} \\
\text{November (0 - 500m a.g.l.)} & f(k) = 1.7e^{-9.08(k-1.18)^2} \\
\text{All Year (0 - 500m a.g.l.)} & f(k) = 1.75e^{-9.62(k-1.21)^2}
\end{array}\right\} \quad (5.2)$$

Table 5.10 Calculated Values of k_e for Botswana from model

Period	k_e
February (0-500m a.g.l.)	0.58
May (0-500m a.g.l.)	0.71
August (0-500m a.g.l.)	0.95
November (0-500m a.g.l.)	0.64
All Year (0-500m a.g.l.)	0.70
All Year (0-200m a.g.l.)	0.61

Table 5.11 Calculated Values of k_e for Durban from model

Period	k_e
February (0-500m agl)	0.20
May (0-500m agl)	0.30
August (0-500m agl)	0.90
November (0-500m agl)	0.50
All Year (0-500m agl)	0.50

5.7 Discussion and Conclusion

The overall median value of k for Botswana is 1.12, with a k_e = 0.7 for 0-500m a.g.l. and k_e = 0.61 for 0-200m a.g.l. On the other hand, the corresponding values for Durban are median k = 1.21 and k_e = 0.5. The differing features of Durban and Botswana (Maun) are: Durban has a higher pressure (P ~ 1015 hpa), while that of Maun is about 910 hpa at ground level. The temperatures are very high for Botswana (up to 30°C in November and February), while they are much lower for Durban (about 24°C in November and February). The water vapour pressure for Botswana is about 10hpa (November and February) while for Durban it is about 24 hpa (November and February). The corresponding refractivity values are 370 N-units in February for Durban, 360 N-units in November. For Botswana, the corresponding values are 270N-units for February and November. Noting that:

$$\frac{dN}{dh} = 77.6\frac{1}{T}\frac{dP}{dh} - \left(\frac{77.6P}{T^2} + \frac{746{,}512e}{T^3}\right)\frac{dT}{dh} + \frac{373{,}256}{T^2}\frac{de}{dh} \qquad (5.3)$$

We see that the temperature T has the largest effect on dN/dh (note: dN/dh is negative in general). Hence for Botswana, since T is larger, the variation dN/dh is smaller (but negative) than for Durban. Therefore, the denominator of k is lower for Durban (median k is 1.21) than for Botswana (median k is 1.12)(equation 2.27). dN/dh is relatively higher in winter than in summer,

since T is lower in winter than in summer. But dN/dh is negative with a magnitude much less than 1.

Since for both Durban and Botswana, the month of August is the winter month, the temperature T is lowest for the year. Therefore dN/dh would be highest in winter (than in summer) and hence the denominator of k will be lowest in this season. Hence k is observed to have the highest value in the winter months of August for both Botswana and Durban. On the other hand, the summer month of February has the highest temperature T for the year; hence dN/dh would therefore be highest for the month and k is observed to be lowest for the summer months of February. Thus, for Botswana mean k = 1.08 in February, while, for Durban, median k = 1.12 for February. These are found to be the lowest for the whole year. Baker and Palmer, on the other hand, have a value of k = 1.46 for Durban.

For Botswana, k is highest in August (median k = 1.14, k_e = 0.95). The standard deviation, σ is lowest (σ = 0.0665), which implies a very narrow distribution of k for the month. One observes a similar situation in Durban, in August with the highest value of k found (median k = 1.26, k_e = 0.90). The corresponding standard deviation is also lowest in August (σ = 0.1078).

CHAPTER SIX

6.1 Application of Effective Earth-Radius Factor

Effective earth radius factor (the k-factor) has major applications in the design of terrestrial line-of-sight links. Hence, depending on the frequency of propagation, different values of k-factor can be implemented for operational purposes [9]. The most frequently used value of k is 4/3. Telkom South Africa uses a k-factor of 4/3 while transmitting at frequencies of 38 GHz, 23 GHz and 13GHz in the U8 (Upper 8) MHz and U7- MHz [24]. They use these bands in the microwave planning while transmitting at power levels just below 1W depending on the stability of the system and interference is managed by proper network and frequency planning.

6.2 Link Design Costing

The link design process described in chapter two could be costed so that one can verify what is actually obtainable in the industry e.g. Telkom South Africa. Below is a scenario of costing a simple radio link design. The link cost is basically for equipment to connect the link, hence, the cost of mast or tower height is not included. Investigation shows that a 55-meter tower costs R450, 000.00, giving the cost per meter to be about R8,200 (this includes the base, support costing and earthing). The total cost would therefore be the equipment cost plus the cost of tower depending on the tower height for the link in question. Table 6.1 shows the cost of equipment to terminate the link at the transmitting and receiving stations. The tower height can be calculated using the procedure in Chapter two.

A scenario is set up say for a link between Sherwood and Umlazi in KwaZulu-Natal Province of South Africa. The link, transmits at a frequency of 23 GHZ, with an effective earth radius factor of 4/3. The path length between the transmitting and receiving station is determined to be 48.28 km. The tower height at Sherwood (the transmitting station) is fixed at 60m (see Fig. 6.1).

The cost of this tower will approximately be:

$$R8{,}200 * 60m = R492{,}000.00$$

Table 6.1 Cost of Equipment to Setup a Radio Link [22]

Equipment Type Asset Description (80)	**Qty**	**Unit Cost R**	**Planned Total Cost R**
8a3 outdoor link set	1	75,873.00	75,873.00
8 GHz 0.6 m int antenna	2	18,013.00	36,026.00
Flexible coaxial cable (per m)	94	0.72	67.68
4x2 mbit/s QPSK link set	1	42,045.00	42,045.00
Outdoor inst/re-inst	1	680.50	680.50
Indoor inst/re-inst	1	1,993.98	1,993.98
Minor material	1	11,243.31	11,243.21
		ASSET TOTAL	**167,929.37**

After the obstruction clearance of 60%, the tower height at the Umlazi (the receiving station) is 88 m (see Fig. 6.1). The receiving tower cost is now calculated approximately as follows:

$$R8{,}200 * 88m = R721{,}600$$

Hence, the total tower cost for both side of the link is approximately

$$R492{,}000 + R721{,}600 = R1{,}213{,}600$$

Finally, adding this to the initial equipment costing above, we have

$$R1{,}213{,}600.00 + R167{,}929.37 = R1{,}381{,}529.37$$

Using the k value of 1.21 for Durban, in this same scenario we have the following results. The tower height at Sherwood was maintained at the same height as before i.e. 60m and the cost remains same for this end of the link.

After the obstruction clearance of 60%, the tower height at Umlazi is now observed to be 90m, (see Fig. 6.2). The cost of the receiving end tower with this k value is calculated as follows:

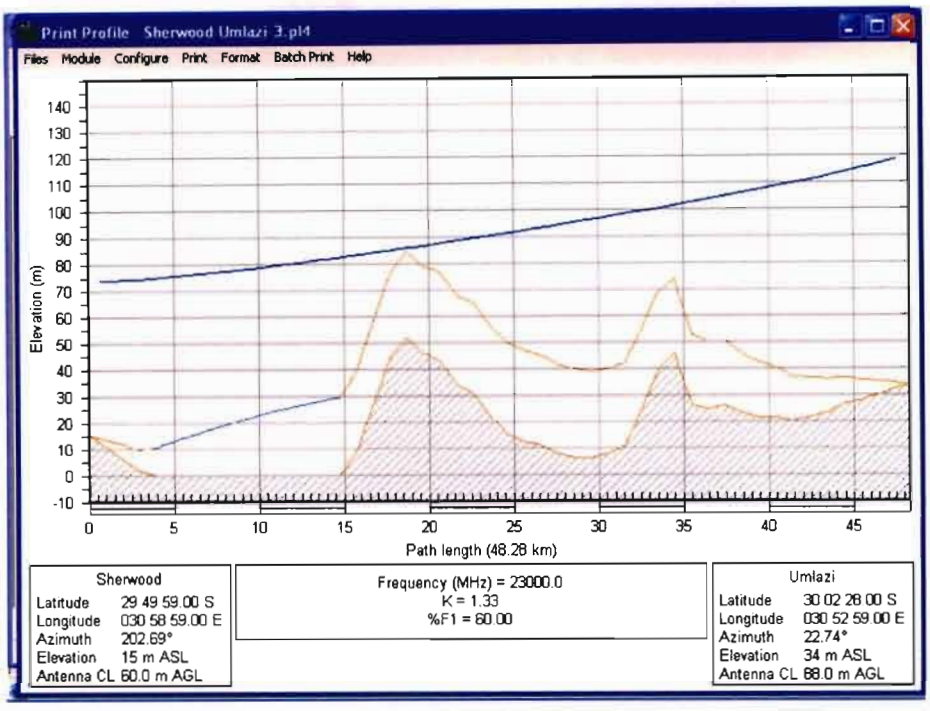

Fig. 6.1. Path Profile Diagram for Radio Link between Sherwood and Umlazi at k = 1.33

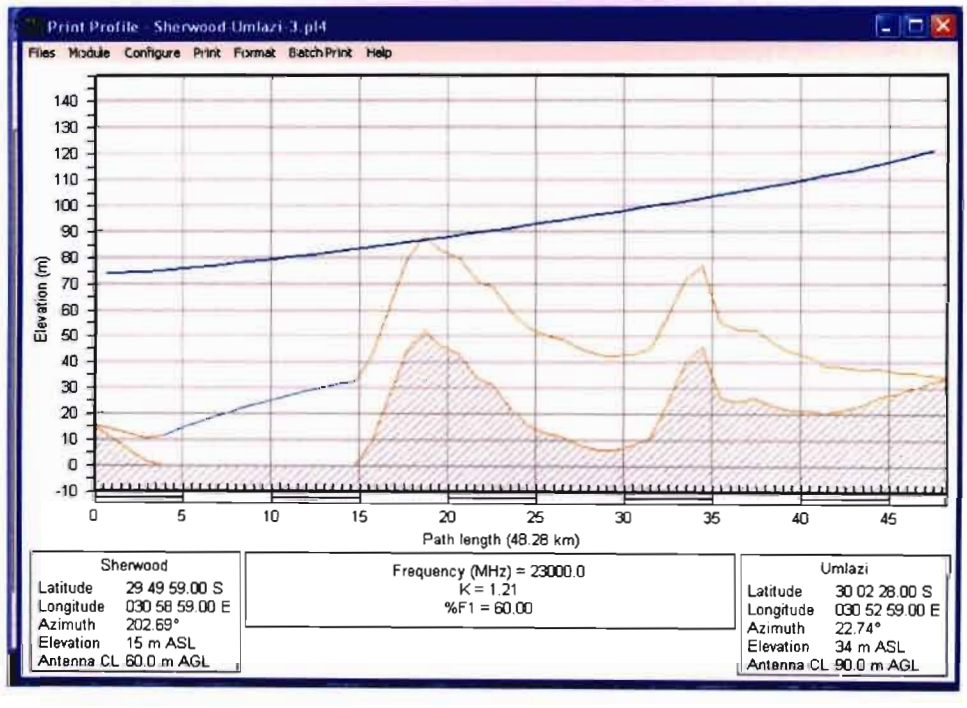

Fig. 6.2. Path Profile Diagram for Radio Link between Sherwood and Umlazi at k = 1.21

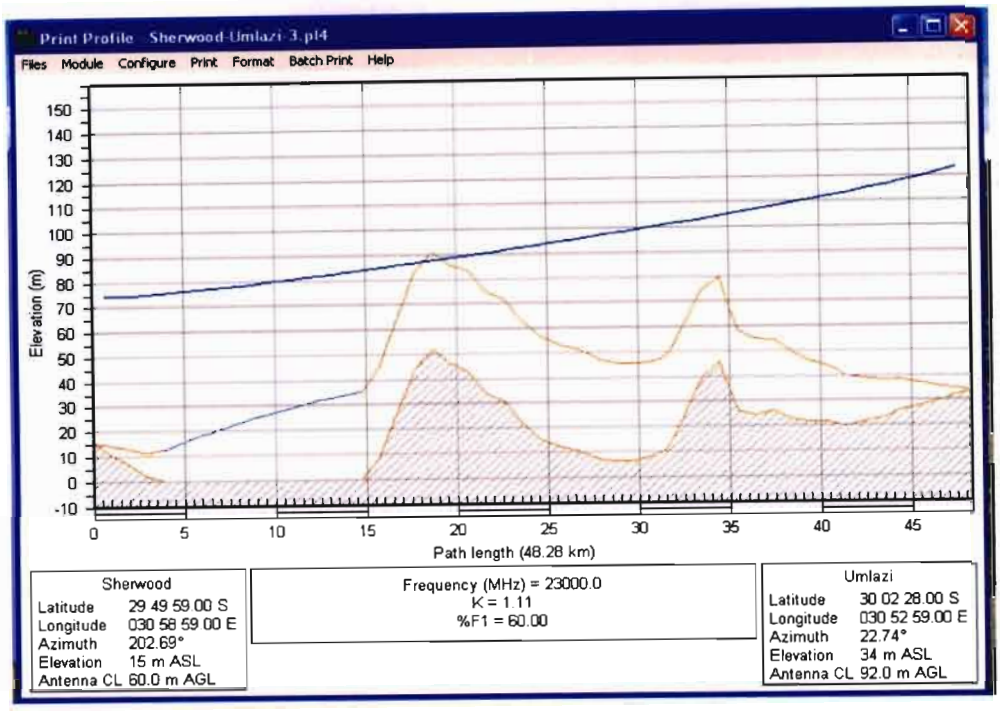

Fig. 6.3. Path Profile Diagram for Radio Link between Sherwood and Umlazi at k = 1.11

$$R8{,}200 * 90m = R738{,}000$$

Hence, the total tower cost for both side of the link is approximately:

$$R492{,}000 + R738{,}000 = R1{,}230{,}000$$

Finally, adding this to the initial equipment costing above, we have

$$R1{,}230{,}000.00 + R167{,}929.37 = R1{,}397{,}929.37$$

The path profile for different values of k are plotted and included. Similar conclusions can be drawn by using k =1.1, k = 1.0, and k = 0.6 (figures 6.3 – 6.5).

6.2.1 Applying the Knife-edge Diffraction Loss in Link Design

Applying the diffraction effects discussed in section 2.5, the Fresnel radius for the link above is calculated below using equation (2.6) and (2.25a) assuming a transmitting frequency of 23 GHz (for short-hop radio links).

Frequency f = 23 GHz, c = 3 x 10^8

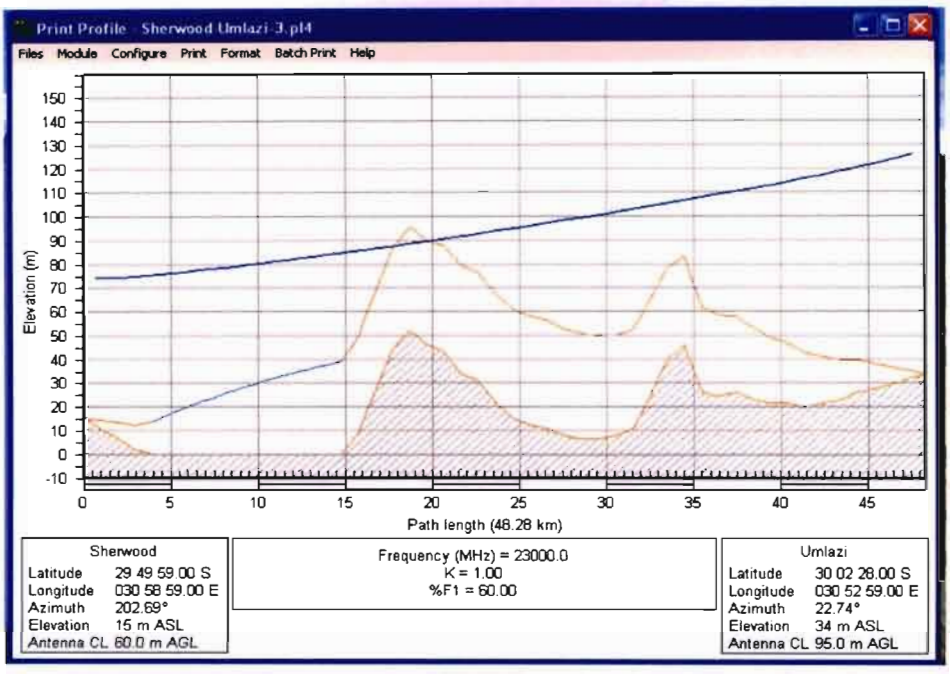

Fig. 6.4. Path Profile Diagram for Radio Link between Sherwood and Umlazi at k = 1.00

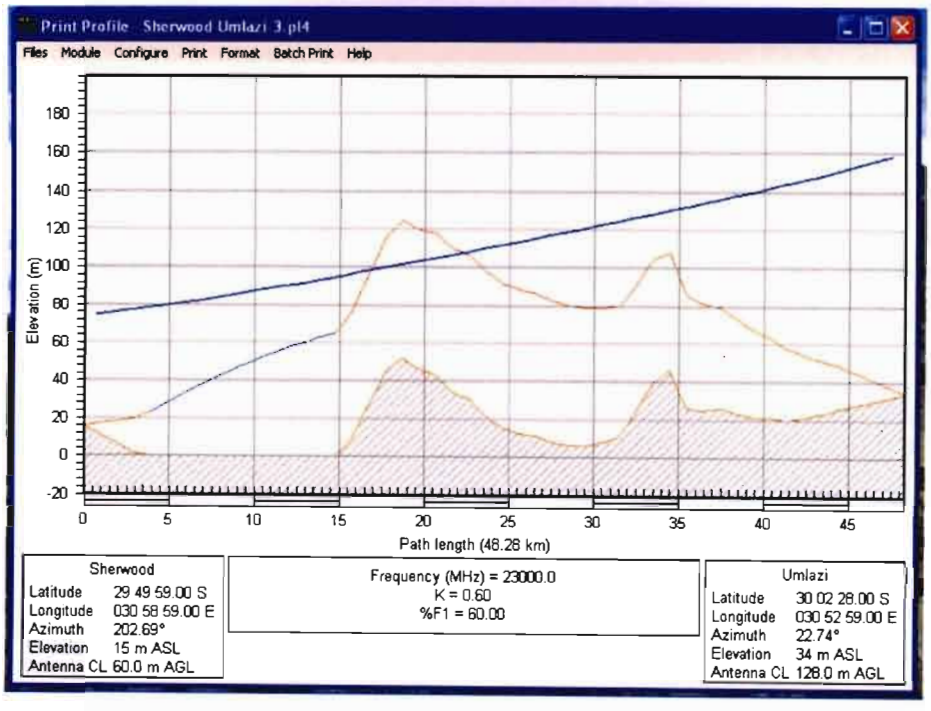

Fig. 6.5. Path Profile Diagram for Radio Link between Sherwood and Umlazi at k equal 0.6

$$c = f\lambda$$

$$\lambda = \frac{c}{f} = \frac{3x10^8}{23x10^9}$$

$$\lambda = 0.013m$$

Hence

$$r_f = \sqrt{\frac{\lambda d_1 d_2}{d_1 + d_2}}$$

$$r_f = \sqrt{\frac{0.013x18x10^3 x30.28x10^3}{48.28}}$$

$$rf = 12.1$$

Clearing 60% of the Fresnel radius.

$$0.6r_f = 0.6x12.1 = 7.268m$$

Table 6.2 shows the effect of different values of k and the obstruction caused by these values into the Fresnel zone radius above 60% clearance.

Table 6.2 The k-factor Variation with Obstruction values and Umlazi Tower Height (to clear 60% r_f)

k	Obstruction Δh in m (w.r.t k = 4/3)	Tower Required Height (Umlazi) in m
1.33	0	88
1.22	-3	90
1.21	-3	90
1.11	-6	92
1.00	-10	95
0.9	-15	98
0.8	-21	100
0.7	-27	105
0.6	-39	128

Where Δh is the excess obstruction at point (d_1 = 18, d_2 = 30.28) above k = 4/3.

Using the design value of k = 4/3, one can use table 6.2 above to calculate the diffraction loss parameters h, v, and G_d(dB) using equation (2.35) of chapter two as follows:

$$for\ k = \frac{4}{3},$$

$$h = -7.268 - \Delta h$$

$$h = -7.628 - 0$$

$$h = -7.628$$

$$v = h\sqrt{\frac{2(d_1 + d_2)}{\lambda d_1 d_2}}$$

$$v = -7.628\ x\sqrt{\frac{2(48.28x10^3)}{0.013x18x10^3 x30.28x10^3}}$$

$$v = -7.268\ x\ 0.1167$$

$$v = -0.84845$$

$$G_d\,(dB) = 20\log(0.5 - 0.62v)$$

$$G_d\,(dB) = 20\log(0.5 - 0.62x - 0.84845)$$

$$G_d\,(dB) = 0.2233\ dB$$

Similar procedure as above is used with different values of k and the results obtained are tabulated in Table 6.3 below:

Table 6.3 Effect of the k-factor variation on Diffraction Gain

k	h	v	G_d (dB)
1.33	-7.268	-0.84845	0.2233 dB
1.2	-4.268	-0.49807	-1.843 dB
1.1	-1.268	-0.1479756	-4.557 dB
1.0	2.732	0.3188	-8.6512 dB
0.9	7.732	0.90232	-15.165 dB
0.8	13.732	1.60252	-17.379
0.7	19.732	2.3027	-20.8968
0.6	31.732	3.7031	-24.32766

With k = 4/3, if the link between Sherwood and Umlazi has a design availability of 99.99%, the required fade margin for k = 4/3 is 38dB. However, when the link is installed between Sherwood and Umlazi and actual k = 1.21, the fade margin degrades by 1.843 dB to 36.157 dB (Table 6.3). This therefore reduces the link availability to 99.97%.

On the other hand, for Botswana, where median k = 1.12, the fade margin on a similar link would be reduced by 4.56 dB; therefore the link availability would be about 99.95%. This statement highlights the consequence of radio design using inappropriate values of k.

CHAPTER SEVEN

7.1 Conclusion

The importance of an accurate prediction of effective earth radius factor (the k-factor) cannot be overemphasised in radio communication studies. In this report, the k-factor distribution for Southern Africa has been studied. A proposed model for the pdf distribution of the k-factor for Southern Africa was given. The two countries chosen for case study are Botswana and South Africa. Radiosonde data collected over a three-year period in Maun, Botswana was used as part of the model formulation data, also radiosonde data collected over a period of ten months from Durban Weather Station (station number: 68588) via the South African Weather Service [11] was also used in the study.

For Botswana, for the height ranges 0-200m and 0-500m a.g.l., the median k value of 1.12 is observed. The value 0f $k_e = 0.70$ was observed for the height range of 0-500m while for the height range of 0-200m agl, a k_e value of 0.61 was noted. The k_e value was observed to be lowest in summer for Botswana (with an effective value of 0.58 in February) (See Table 5.10) while it was highest in winter with a value of 0.95 in August (See Table 5.10).

In South Africa, the median value of k is found to be 1.21 for the height range of 0-500m agl. Meanwhile earlier work of Baker and Palmer predicted the median ground-level k value to be 1.46 for Durban at a height of 8m. The discrepancy in our result and theirs might not be unconnected with the differences in height ranges. The effective k value for Durban was found to be lowest in summer with a value of $k_e = 0.2$ in February (See Table 5.11) while it was highest in winter with $k_e = 0.5$ in August (See Table 5.11).

It is noted that the higher temperature range for Botswana results in the lower median k value compared to Durban with a lower temperature range. This fact also determines why k value is lower in winter than in summer, as shown for both Botswana and Durban.

The application of the study was done using a simple scenario setup for a 48.28 km link between Sherwood and Umlazi in KwaZulu-Natal Province of South Africa, the knife-edge diffraction model described in Chapter two was applied. The design value of $k = 4/3$ was initially used in

the application; the actual value of 1.2 was then used. Similar scenario was applied to Botswana using the actual value of k = 1.12 for Botswana.

It is noted that the fade margin degrades from 38 dB (when the design value of $k = 4/3$ is used) to 36.1 dB (for k = 1.21). A similar scenario set up for Botswana reduced the fade margin by 4.5 dB for the link. Hence, it can be concluded that using the actual value of k for a link design in a given location will increase the quality of the transmitted signal, enhance system performance and increase link reliability.

7.2 Recommendation for Future Work

The sites for data collection should be expanded for South Africa; more reference stations rather than Durban alone need to be included for future studies. This will give a more detailed study for the k-factor distribution in South Africa.

Radiosonde that reports after every two seconds of ascent should be acquired for future studies. The one used in this study reports after every ten seconds of ascent, which translates into 50m height intervals.

Due to financial constraint involved in obtaining a radiosonde since its very expensive, ground data which can be gathered more easily should be used for future studies. The data should cover a much longer period.

REFERENCES

[1] T. J. Afullo, M.O. Adongo, T. Motsoela and F. Molotsi "A Study of Radio Refractivity and Super-Refractivity in Botswana", Transactions of South Africa institute of Electrical Engineers (SAIEE), vol. 90, June 1999, pp 61-68.

[2] T.J. Afullo, M.O Adongo, T. Motsoela "Seasonal Variation of Radio Refractivity in Botswana", Proceedings of the URSI Commission F Open Symposium on Climatic Parameters in Radiowave Propagation Prediction, (CLIMPARA '98) Ottawa, Canada, 27-29, April 1998, pp 195-198.

[3] G.P. Brasseur, John J. Orlondo and G.S. Tyndall "Atmospheric Chemistry and Global Change", New York , Oxford University Press, 1999, Chapter One.

[4] Thomas A. Blair "Weather Element" Prentice-Hall, Inc. Eaglewood Cliffs, N.J. 1957, pp 7-30, chapters one and two.

[5] D.C. Baker and A.J. Palmer "Predicting the Long-term Average of the Effective Earth Radius Factor for South Africa using ground-based observations", presented at the IEEE region 8 Conference in Gaborone, 15-17 September, 2004, vol. 2, 2004, pp 1003-1006.

[6] D.C. Baker and A.J. Palmer "Predicting the Monthly Cumulative Distribution of the Effective Earth Radius Factor for South Africa", Presented at the IEEE Region 8 Conference Gaborone, Botswana, 15-17 September, 2004, vol. 2, pp 1007-1010.

[7] R.L Olsen "Radioclimatological Modeling of Propagation Effects in Clear-Air and Precipitation Conditions: Recent Advances and Future Directions", Proceedings of the third Regional Workshop on Radio Communications in Africa, (Radio Africa '99) Gaborone, Botswana, October 1999, pp 93-106.

[8] T.J. Afullo and P.K. Odedina "Effective Earth Radius Factor Characterisation for Line-of Sight Paths in Botswana", presented at IEEE region 8 Conference, Gaborone, Botswana, 15-17 September, 2004, vol.1, pp 227-231.

[9] Roger L. Freeman, "Radius System Design for Telecommunications (1-100 GHZ)", Publisher John Wiley and sons Inc. USA, 1987, pp1-25, 32-34.

[10] ITU Radiocommunication Assembly: "Propagation data and Prediction Methods for the Design of Terrestrial Line-of-Sight Systems", Geneva, Switzerland Document No. ITU-R P.530-10, 2001.

[11] Amith S. Dabideen "Radio Refractivity Measurement for KwaZulu-Natal", Msc dissertation submitted to the Department of Electrical Engineering, University of KwaZulu-Natal (Westville Campus), pp 53, 99-120, November 2004.

[12] D.C Baker and A.J Palmer "A Proposed Empirical model of the Effective Radius Factor for Telecommunications use in South Africa", presented at the IEEE region 8 (AFRICON '02) Conference, George, 2-4 October, 2002.

[13] D.C Baker and A.J Palmer, "A Model for the Fraction of time Availability of the Effective Earth Radius Factor for Communications Planning in South Africa: Part I – The basic model", Transactions of SAIEE, 2002, vol. 93, No 1, pp 1-7.

[14] D.C Baker and A.J "A Model for the Fraction of time Availability of the Effective Earth Radius Factor for Communications Planning in South Africa: Part II – Inclusion of climatic term", Transactions of SAIEE, 2002, vol. 93, No 3, pp 129-134.

[15] E.C. Jordan "Electromagnetic Waves and Radiating Systems", Prentice Hall, International, 1968.

[16] Donald H. Hamsher . " Communication System Engineering Handbook" McGraw-Hill, Inc. 1967,pp 16-30 – 16-40.

[17] T.S. Rappaport, "Wireless Communications Principle and Practice", Prentice Hall PTR Upper Saddle River, N.J. 07458, 1996, pp 91-97.

[18] Carlos Salema " Microwave Radio Links from Theory to Design" John Wiley and Sons, Inc., New Jersey, 2003, pp 89-91.

[19] T.J Afullo, M.O. Adongo, T.Motsoela and D.F. Molotsi, "Estimates of Refractivity Gradient and k-factor Ranges for Botswana", Transactions of South Africa institute of Electrical Engineers (SAIEE), vol.92, pp 1-6, 2001.

[20] R.L. Olsen and Terje Tjelta "Worldwide Techniques for Predicting the Multipath Fading Distribution on Terrestrial LOS Links: Background and Results of Tests", IEEE Transactions on Antennas and Propagation, vol. 47, No 1, January 1999.

[21] Andrew Martin "Key Radio Meteorological Parameter for Detecting Line-of-Sight Links in a Multipath Fading Environment", Martin Communications pty Ltd, 87 Peter Avenue, Mulgrave, VIC 3170, Australia.

[22] T.G Hayton, S.L. Lystad, A.K. Marsh, K.H. Craig "Characterisation of Clear-Air Parameters derived from High Resolution Radiosondes", in Proceedings of the URSI Commission F Open symposium on Climatic Parameters in Radiowave Propagation prediction, Ottawa, Canada, April 1998, pp 1-8.

[23] G.O. Ajayi "Physics of Tropospheric Radiopropagation", presented at the 2nd Regional Workshop on Development of Radio Communication in Africa, 4-8 August, 1997, KCCT, Nairobi, Kenya, pp 43-72.

[24] C.A. Alais, M.L. Keller, T.E. Pistorious, P.J Smith Procedure for Link Design for Point to Multipoint (Terrestrial Wireless Systems), November 1998, pp 51-79.

[25] M.O. Ajewole, L.B. Kolawole, G.O. Ajayi, "Effects of Variation in Raindrop size Distribution for Different Rain Types on Attenuation and Phase Shift of Microwave Signals in Nigeria" in Proceedings of the URSI Commission F Open symposium on Climatic Parameters in Radiowave Propagation prediction, Ottawa, Canada, April 1998, pp 155-158.

[26] Unpublished Data from South African Weather Service for November 2003 – August 2004 (See also [11]).

[27] Unpublished Data from Department of Meteorological Services, Gaborone, Botswana for 1996 – 1998 (See also [1]).